A Lin's method approach to finding and continuing heteroclinic connections involving periodic orbits

Bernd Krauskopf[1] **and Thorsten Rieß**[2]

[1]Department of Engineering Mathematics, University of Bristol, University Walk, Bristol BS8 1TR, UK

[2]Faculty of Mathematics and Natural Sciences, Technische Universität Ilmenau, Pf 100565, 98684 Ilmenau, Germany

November 2007

Abstract. We present a numerical method for finding and continuing heteroclinic connections of vector fields that involve periodic orbits. Specifically, we concentrate on the case of a codimension-d heteroclinic connection from a saddle equilibrium to a saddle periodic orbit, denoted EtoP connection for short. By employing a Lin's method approach we construct a boundary value problem that has as its solution two orbit segments, one from the equilibrium to a suitable section Σ and the other from Σ to the periodic orbit. The difference between their two end points in Σ can be chosen in a d-dimensional subspace, and this gives rise to d well-defined test functions that are called the Lin gaps. A connecting orbit can be found in a systematic way by closing the Lin gaps one-by-one in d consecutive continuation runs. Indeed, any common zero of the Lin gaps corresponds to an EtoP connection, which can then be continued in system parameters.

The performance of our method is demonstrated with a number of examples. First, we continue codimension-one EtoP connections and the associated heteroclinic EtoP cycles in the Lorenz system. We then consider a three-dimensional model vector field for the dynamics near a saddle-node Hopf bifurcation with global reinjection to show that our method allows us to complete a complicated bifurcation diagram involving codimension-one EtoP connections. With the example of a four-dimensional Duffing-type system we then demonstrate how a codimension-two EtoP connection can be found by closing two Lin gaps in succession. Finally, we show that our geometric approach can be used to find a codimension-zero heteroclinic connection between two saddle periodic orbits in a four-dimensional vector field.

AMS classification scheme numbers: 34C37, 37M20, 65L10, 34C60

1. Introduction

Vector fields arise as mathematical models of choice in numerous application areas; see, for example, textbooks such as [19, 25, 37] as entry points to the extensive literature. To determine the possible dynamics of a vector field under consideration one needs to find the attracting, repelling and saddle-type compact invariant objects, in particular, equilibria and periodic orbits, together with the stable and unstable manifolds of the saddle-type objects. The global dynamics can then be determined from the arrangement of stable and unstable manifolds and how it changes with parameters. Important in this context are homoclinic and heteroclinic orbits, which

arise as intersection curves between stable and unstable manifolds of the same or of two different saddle objects. As such, they are also referred to as global or connecting orbits. One associates a codimension with a connecting orbit by saying that it is of codimension d if it generically exists at isolated points in d-dimensional parameter space; here, a codimension-zero connecting orbit refers to a robust intersection of the respective stable and unstable manifolds. It is now well established that connecting orbits are closely related to significant changes of the global dynamics, including the appearance of chaotic dynamics; see again [19, 25, 37]. Furthermore, heteroclinic cycles of codimension $d \geq 1$ may act as organizing centres for the dynamics, meaning that their study allows conclusions on the qualitative dynamics nearby. Therefore, it is crucial to find and follow them in system parameters. Due to the global nature of connecting orbits, this task generally requires the use of advanced numerical methods.

The development of numerical methods for the continuation of homoclinic and heteroclinic orbits has been an active field of research [3, 4, 5, 11, 12, 18, 23, 26]. Today, homoclinic and heteroclinic orbits to equilibria can readily be continued, for example, with the HomCont [5] part of the well-known continuation package Auto [15]. The underlying idea is to represent the connecting orbit as the solution of a boundary value problem over a finite time interval by imposing projection boundary conditions, which ensure that the two endpoints lie in the stable and unstable eigenspaces of the respective equilibria; see, for example, [4, 12]. This makes it possible to explore and understand complicated bifurcation diagrams involving homoclinic and heteroclinic orbits to equilibria; recent examples include the study of global bifurcations in a semiconductor laser system [40] and in models of calcium dynamics in cells [6].

This paper is concerned with the next logical step: the continuation of connecting orbits involving saddle periodic orbits. One distinguishes two types of such orbits: connections from a saddle equilibrium to a saddle periodic orbit, which we refer to as *EtoP connections*, and heteroclinic connections between the same or two different periodic orbits, or *PtoP connections* for short. Codimension-one EtoP connections are of particular relevance, because their existence can be inferred from the occurence of certain codimension-two bifurcations of connections to equilibria. An example is a Shilnikov-Hopf bifurcation where the saddle focus involved in a codimension-one homoclinic orbit undergoes a Hopf bifurcation; see [6, 20, 40]. Another example is the possibility that homoclinic bifurcations of a saddle equilibrium may accumulate on a heteroclinic EtoP cycle of an equilibrium and a saddle periodic orbit. This phenomenon was studied theoretically in [33] and then found near a saddle-node Hopf bifurcation with a global reinjection mechanism [22].

We present here a Lin's method approach to finding and continuing heteroclinic connecting orbits involving periodic orbits. We concentrate on the case of codimension-d EtoP connections, but our approach can also be applied to PtoP connections. Lin's method [28] is an analytical theory that can be used to analyze the recurrent dynamics near, for example, homoclinic orbits or heteroclinic cycles; see also [21, 33, 34, 35, 41]. The main result in the present context is that for any value of the system parameter there are two well-defined orbit segments from the equilibrium to a suitable section Σ and from Σ to the periodic orbit, whose difference lies in a d-dimensional subspace; see section 2 for details. This gives rise to d well-defined test function, which are also called the Lin gaps. The sought-after codimension-d EtoP connection can then be found by closing each of the Lin gaps one by one via suitable continuation runs. The two orbit segments are represented as solutions of a boundary value problem subject to projection boundary conditions. Near the equilibrium we use a well-

established condition [4] as implemented in HomCont [5], while the projection boundary condition near the periodic orbit is adapted from the method in [17]. All boundary value problems are solved with the continuation package Auto in the flavours Auto2000 [15] and Auto07p [16]. Once a codimension-d EtoP connection has been detected as a common zero of the d test functions, it can readily be continued in additional system parameters. Furthermore, by considering the corresponding EtoP heteroclinic cycle, other global orbits that bifurcate from it, for example, a codimension-zero homoclinic orbit of the periodic orbit, can be found and continued as well.

A number of other methods for the continuation of EtoP and PtoP connections have been proposed recently [3, 9, 13, 32]. They have in common that the connecting orbit is represented as *a single orbit segment* over a finite time interval by imposing suitable boundary conditions at the periodic orbit. A common difficulty is that of finding an initial approximate connecting orbit that satisfies the boundary value problem. The seminal work by Beyn [3] introduces a general setup in terms of suitable projection boundary conditions and establishes corresponding error bounds. Pampel [32] further analyses and implements the EtoP connection scheme and uses it to compute the codimension-one EtoP connection in the Lorenz system; here an initial connecting orbit is obtained by continuation (in a system parameter) of intersection curves of the stable and unstable unstable manifold in a suitably chosen plane. Dieci and Rebaza [9, 10] follow the general approach of [3] and combine it with the method of continuing invariant subspaces from [7] to formulate the boundary conditions at the equilibrium and the periodic orbit. They compute and continue in parameters the codimension-one EtoP connection in the Lorenz system and a codimension-zero PtoP connection in a coupled oscillator system; in both cases, a simple shooting method is used to find an initial connecting orbit. Finally, Doedel *et al.* [13] present an implementation for EtoP connections, where the adjoint variational equation along the periodic orbit is used to formulate projection boundary conditions. As examples they continue codimension-one EtoP connections in the Lorenz system, in a three-dimensional model of an electronic circuit, and in a three-dimensional food-chain model. Doedel *et al.* use a homotopy-type method to find an initial connecting orbit. They start by continuing an orbit from near the equilibrium in the unstable eigenspace to find an intersection point with the stable eigenspace of the periodic orbit. The distance of this intersection point to the periodic orbit is then reduced in additional continuation steps. This homotopy approach works well when the (un)stable manifold of the equilibrium is of dimension one and the dimension n of the phase space is not too large. However, it requires that one starts quite close to the EtoP connection, and it is less systematic when two-dimensional manifolds are involved.

The main property of our method is that it uses *two separate orbits segments* up to a suitably chosen section as a means of setting up a systematic way of finding codimension-d EtoP connections for any $d \geq 1$ and for arbitrary dimensions of the stable and unstable manifolds of the equilibrium and periodic orbit involved. Namely, one chooses the section Σ to divide the phase space into two regions, one of which contains the equilibrium and the other the periodic orbit (for parameters chosen from a region of interest). Then any EtoP connection will intersect Σ and, generically, this intersection is transverse. Therefore, the boundary value problem for the two orbit segments that define the Lin gaps can has a unique solution in a (generally large) region of parameter space, and not just at the EtoP connection itself. The Lin gaps are well-defined test functions in this entire region, and any common zero corresponds

to an EtoP connection. In particular, if no common zero can be found then the sought-after EtoP connection does not exist in the considered parameter region. Conversely, it is possible that several common zeros are found, which then correspond to different EtoP connections. Note that our approach is similar in spirit to the implementation of Lin's method in [31], where regular test functions are set up that allow one to switch branches from a known homoclinic orbit (to an equilibrium) to nearby n-homoclinic orbits that pass close to the equilibrium $(n-1)$ times before returning back to it.

The performance of our method, and its use as a stepping stone for the study of complicated bifurcation diagrams with EtoP connections, is discussed in detail with three examples in section 4. In section 4.1 we find the codimension-one EtoP heteroclinic cycle of the origin in the Lorenz system, which consists of a codimension-one EtoP connection and a codimension-zero EtoP connection from the periodic orbit back to the origin. The entire EtoP heteroclinic cycle is then continued in two parameters. We also demonstrate how the continuation of a codimension-zero homoclinic orbit to the periodic orbit can be started from the data for the EtoP cycle. Section 4.2 is a thorough investigation of EtoP connections and associated global bifurcations in the three-dimensional model vector field from [22] for the dynamics near a saddle-node Hopf bifurcation with a global reinjection mechanism. This reveals the bifurcation phenomena behind the accumulation of a curve of homoclinic orbits (to an equilibrium) on a curve of codimension-one EtoP connections. Successive maxima and minima of this accumulation process appear close to curves of tangencies that bound a region where the codimension-zero connection of the overall EtoP cycle exists. This completes the study in [22] in agreement with the theoretical results in [33]. What is more, we detect and continue a second EtoP connection, which reveals a new accumulation phenomenon: the EtoP connection itself accumulates on a segment of a curve of the first EtoP connection. In the process, a codimension-zero homoclinic orbit to the periodic orbit 'splits off'. Our results suggests that the accumulation of a connecting orbit onto a curve segment is quite a general mechanism. Finally, section 4.3 is an example that shows that our method also works for EtoP connections of a higher codimension. Namely, we find and continue a codimension-two EtoP connection in a four-dimensional Duffing-type system, which involves closing two Lin gaps in succession.

This paper is organized as follows. Section 2 gives the analytical background information of Lin's method as needed for finding EtoP connections. The implementation of our method, with the list of all relevant boundary conditions, can be found in section 3. How it can be used in practise is illustrated at length in section 4. Section 5 discusses how our geometric approach can be generalized to PtoP connections and we show how a codimension-zero PtoP connection in a four-dimensional system can be found. Finally, in section 6 we summarize and discuss directions of future research.

2. Lin's method for an EtoP connection

To fix notation, we consider a vector field

$$\dot{x} = f(x, \lambda), \tag{1}$$

where

$$f : \mathbb{R}^n \times \mathbb{R}^m \to \mathbb{R}^n \tag{2}$$

is sufficiently smooth; for simplicity we assume throughout that f is at least twice differentiable. Here $\mathbb{R}^n$ is the phase space of (1) and $\lambda \in \mathbb{R}^m$ is a multi-dimensional parameter. We denote the flow of (1) by ϕ^t. Note that all objects involved (equilibrium, periodic orbit, their invariant manifolds, etc) dependend on λ, but we generally do not indicate this explicitely in the notation.

Our main object of study is an EtoP connection, that is, a heteroclinic connecting orbit Q of (1) between a hyperbolic equilibrium p and a hyperbolic periodic orbit Γ at a some parameter value λ^*. For definiteness we assume in the formulation below that the flow along the connection is from p to Γ. (This can always be achieved by a reversal of time in (1) if the flow is in the opposite direction.) More precisely, we assume that the following conditions are satisfied.

(C1) The equilibrium point p is hyperbolic in a neighborhood Λ of λ^* and its unstable manifold

$$W^u(p) := \{x \in \mathbb{R}^n \mid \lim_{t\to-\infty} \phi^t(x) = p \} \tag{3}$$

is of dimension $k \geq 1$.

(C2) The periodic orbit Γ is hyperbolic in a neighborhood Λ of λ^* and its stable manifold

$$W^s(\Gamma) := \{x \in \mathbb{R}^n \mid \lim_{t\to\infty} \mathrm{dist}(\phi^t(x), \Gamma) = 0\} \tag{4}$$

is of dimension $l \geq 2$.

(C3) The dimensions of $W^u(p)$ and $W^s(\Gamma)$ add up to at most the phase space dimension n.

(C4) At $\lambda = \lambda^*$ the manifolds $W^u(p)$ and $W^s(\Gamma)$ intersect in the isolated orbit $Q \subset W^u(p) \cap W^s(\Gamma) \subset \mathbb{R}^n$ and satisfy the genericity condition

$$\dim\left(T_q W^u(p) \cap T_q W^s(\Gamma)\right) = 1 \tag{5}$$

for any point $q \in Q$.

(C5) The dependence of $W^u(p)$ and $W^s(\Gamma)$ on λ is generic, meaning that the λ-dependent families of these manifolds intersect transversely in the product $\mathbb{R}^{n+m}$ of phase space and parameter space.

Note that we do not consider other sources of codimension, such as non-hyperbolicity of p or Γ, or non-transverse interactions of $W^u(p)$ and $W^s(\Gamma)$. We only consider the contribution of the dimension of the intersection of $W^u(p)$ and $W^s(\Gamma)$ as submanifolds of the phase space $\mathbb{R}^n$ to the codimension of Q. Therefore, the codimension of the EtoP connection Q is $d := n+1-k-l \geq 1$, meaning that it is generically encountered if the parameter space is of dimension $m \geq d$.

Our goal is to find the EtoP connection Q for λ^* in a systematic way by starting nearby, that is, in the neighbourhood Λ of λ^*. To formulate our method we now introduce a cross section Σ that intersects Q transversely, which we write as

$$\Sigma = p_\Sigma + Y, \tag{6}$$

where $p_\Sigma \in \mathbb{R}^n$ and Y is an $(n-1)$-dimensional subspace that is most conveniently defined by specifying a normal vector n_Σ. Note that, even when Q is yet unknown, transversality of its intersection with Σ can be achieved by making sure that the flow ϕ^t is transverse to the relevant part of Σ throughout Λ. While the choice of section Σ is effectively arbitrary, it is in the spirit of the method to choose Σ far from p and far from Γ.

Due to transversality of Q and Σ, for all $\lambda \in \Lambda$ we can find (λ-dependent) orbit segments

$$Q^- = \{q^-(t) \mid t \leq 0\} \subset W^u(p) \tag{7}$$

from p to Σ, and

$$Q^+ = \{q^+(t) \mid t \geq 0\} \subset W^s(\Gamma) \tag{8}$$

from Σ to Γ. In other words, $q^-(\cdot)$ and $q^+(\cdot)$ satisfy (1) and the boundary conditions

$$\lim_{t\to-\infty} q^-(t) = p, \tag{9a}$$

$$q^-(0) \in \Sigma, \tag{9b}$$

and

$$\lim_{t\to\infty} \operatorname{dist}(q^+(t), \Gamma) = 0, \tag{10a}$$

$$q^+(0) \in \Sigma, \tag{10b}$$

respectively.

By construction the EtoP connection Q for $\lambda = \lambda^*$ is given as $Q = Q^- \cup Q^+$, which means that Q is characterized by

$$q^-(0) = q^+(0). \tag{11}$$

Since $\dim(W^u(p) \cap \Sigma) = k - 1$ and $\dim(W^s(\Gamma) \cap \Sigma) = l - 1$, equation (11) consists formally of $n - (k-1) - (l-1) = d + 1$ conditions. However, the existence of the EtoP connection Q is only of codimension d, so the task is now to find d well-defined test functions that are zero exactly when (11) is satisfied.

The key idea due to Lin is that the orbit segments Q^- and Q^+ can be chosen in such a way that the difference of $q^-(0)$ and $q^+(0)$ lies in a d-dimensional linear subspace $Z \subset Y$. To define this subspace Z, which is also referred to as the Lin space, we first define the two subspaces

$$W^- := T_{Q\cap\Sigma} W^u(p) \cap Y,$$
$$W^+ := T_{Q\cap\Sigma} W^s(\Gamma) \cap Y.$$

Then Z is defined implicitely by the condition

$$\dim\left(W^+ \oplus W^- \oplus Z\right) = n - 1. \tag{12}$$

Due to the genericity conditions (C3) and (C4) the subspace Z is of dimension d, and we choose basis vectors $z_1, \cdots, z_d$ of Z. Note that there is still an element of choice for Z, which corresponds to the choice of scalar product for which (12) is satisfied. One well-known possibility is that Z is expressed as a linear combination of initial values for bounded (on $\mathbb{R}$) solutions of the adjoint variational equation along Q [35, 21, 31]. We now have all the ingredients to formulate the theorem that is the basis of our method for finding codimension-d EtoP connections. In the literature this is often refered to as the first step of Lin's method; cf. [21].

Theorem 2.1 *Suppose that system (1) has an EtoP connection Q satisfying conditions(C1)–(C5) and let Z be a d-dimensional Lin space satisfying (12). Then there is a neighbourhood Λ of λ^* such that for any $\lambda \in \Lambda$ there are unique solutions Q^- and Q^+ as defined by (7) and (8) that satisfy*

$$\xi(\lambda) := q^+(0) - q^-(0) \in Z.$$

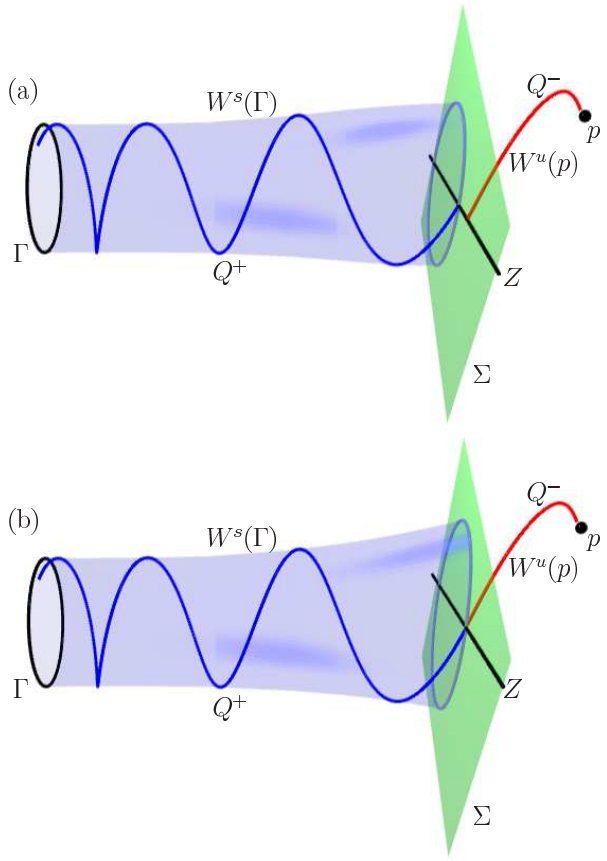

Figure 1. Sketch of the statement of theorem 2.1 in $\mathbb{R}^3$, showing the two-dimensional section Σ and the one-dimensional Lin space Z together with the orbit segments $Q^- \subset W^u(p)$ and $Q^+ \subset W^s(\Gamma)$. Panel (a) shows the situation for λ near λ^*, and panel (b) that for $\lambda = \lambda^*$ where the EtoP connection $Q = Q^- \cup Q^+$ exists.

The proof of theorem 2.1 can be found in [34] for the case $n = 3$ when $\dim Z = 1$. Since the connecting orbit Q is assumed to be generic in the sense of condition (C4), for any n the dimension of Z is d as defined in (C3), that is minimal. Therefore, the proof in [34] generalizes directly to the case $n \geq 3$ considered here. We remark that it is possible to set up Lin's method even if condition (C4) is not satisfied. However, statement and proof for this general case are beyond the scope of this paper and will be reported elsewhere.

As a result of theorem 2.1, for a choice of basis vectors $z_1, \cdots, z_d$ of the Lin space Z there are smooth functions $\eta_i : \mathbb{R}^m \to \mathbb{R}$, $i = 1, \ldots, d$, such that

$$\xi(\lambda) = \sum_{i=1}^{d} \eta_i(\lambda) z_i$$

on the neighbourhood Λ and

$$\eta_i(\lambda^*) = 0 \text{ for all } i = 1, \ldots, d.$$

Due to condition (C5) the matrix $D\xi$ is non-singular. This means that the d smooth functions $\eta_i(\lambda)$ are well-defined test-functions, which we refer to as the Lin gaps.

In light of theorem 2.1, a generic codimension-d EtoP connection Q can be found as follows. After choosing a suitable d-dimensional Lin space Z we can find for a fixed λ near λ^* the unique orbit segments $Q^- \subset W^u(p)$ and $Q^+ \subset W^s(\Gamma)$, such that their difference $\xi(\lambda) = q^+(0) - q^-(0) \in Y$ lies exclusively in the Lin space $Z \subset Y$; recall that $\Sigma = p_\Sigma + Y$ and see figure 1(a) for a sketch of this situation for $n = 3$. The main idea is now to continue the λ-dependent orbit segments Q^- and Q^+ in a suitable combination of system and internal parameters in such a way that the Lin gaps $\eta_i(\lambda)$ become zero one by one. When this has been achieved, we have $\lambda = \lambda^*$ and the EtoP connection Q has been found; see figure 1(b). How this general scheme can be implemented in practice is discussed next.

3. Implementation of the method

For the implementation we formulate the orbit segments Q^- and Q^+ in the form of well-posed boundary value problems, which are then continued with the software package AUTO [15, 16] in suitable parameters to close the Lin gaps. In particular, Q^- and Q^+ need to be truncated to finite time intervals. This can be achieved by using projection boundary conditions [3, 5], where the end points near the equilibrium p and the periodic orbit Γ, respectively, are forced to lie in the local linear eigenspaces. During the continuation both p and Γ need to be continued as discretized objects together with their relevant linearizations. The orbit segments Q^- and Q^+ themselves are represented within the collocation setup of AUTO by Gauss-Legendre polynomials on a variable mesh. As is common, we consider the vector field (1) in the time-rescaled form

$$\dot{u} = T\, f(u, \lambda), \tag{13}$$

where any orbit segment is parameterized over the unit interval $[0, 1]$ and the associated integration time T appears as a separate parameter [11]. In practice, all objects that need to be continued are condensed into one large boundary value problem. We proceed by defining this large system piece by piece. Note that all involved objects depend on the family parameter λ, but for convenience we do not represent this explicitly in the notation.

3.1. Equilibrium and periodic orbit

The equilibrium p simply satisfies the equation

$$f(p, \lambda) = 0 \tag{14}$$

and can be continued in λ as such. We also need to continue the unstable linear eigenspace $E^u(p)$ (which is assumed to be of fixed dimension throughout Λ). In the case that $E^u(p)$ is the span of a single unstable eigenvector, it is often possible to find an explicit formula for it as a function of λ. This has been used in the examples in section 4. More generally, the linearization at p can be continued in λ by extending the system with the eigenvalue problem of the Jacobian (together with a normalization equation for the eigenvector). The eigenspace $E^u(p)$ can then be found for each value of λ. This approach is quite standard and implemented, for example, in the HOMCONT part of AUTO; see [5] for more details.

The periodic solution $\Gamma = \{\gamma(t) \mid 0 \le t \le T_\gamma\}$ is represented as an orbit segment u_γ that satisfies (13) for the (minimal) period $T = T_\gamma$ of Γ, subject to the boundary conditions

$$u_\gamma(0) = u_\gamma(1), \tag{15a}$$

$$\int_0^1 \left\langle \dot{\tilde{u}}_\gamma(\tau), u_\gamma(\tau) \right\rangle d\tau = 0. \tag{15b}$$

Here (15b) is a standard integral phase condition with respect to a reference solution $\tilde{u}_\gamma$ (usually that of the previous continuation step) to ensure that the solution $u_\gamma(\cdot)$ is isolated, so that the boundary value problem for u_γ is well posed [11]. In practice, the numerical representation u_γ of the saddle periodic orbit Γ can be found by continuation, for example, from a known stable periodic orbit or from a Hopf bifurcation of an equilibrium.

Our method requires knowledge of the stable eigendirections of the monodromy matrix of Γ that are associated with the $(l-1)$ stable Floquet multipliers $\mu_1, \ldots, \mu_{l-1}$ of Γ. Each eigendirection corresponds to a solution $\mathrm{v}_i \not\equiv 0$ of the variational equation along Γ that satisfies $\mathrm{v}_i(T_\gamma) = \mu_i \mathrm{v}_i(0)$. Note that the vectors $\mathrm{v}_i(t)$ form a linear bundle along Γ, which is also known as a Floquet bundle.

A numerical representation u_i of the ith stable eigendirection v_i can be obtained as the solution of the boundary value problem

$$\dot{u}_i(t) = T_\gamma D_u f(u_\gamma(t), \lambda) u_i(t), \tag{16a}$$

$$u_i(1) = \mu\, u_i(0), \tag{16b}$$

$$\langle u_i(0), u_i(0) \rangle = h, \tag{16c}$$

where u_γ represents the periodic orbit Γ of period T_γ as above; see [17, 8]. The idea is to start from the trivial solution $u_i \equiv 0$ for $\mu = 0$ and $h = 0$. Continuation in μ results in a branch point at each Floquet multiplier $\mu = \mu_i$. Now one can switch the branch by continuing in the internal parameter h while fixing $\mu = \mu_i$. Note that (16c) is a normalization that uniquely determines u_i, and we stop the continuation when $h = 1$ is reached. Each stable eigendirection u_i $(i = 1, \ldots, l-1)$ can now be continued in the system parameter λ as a solution of (16a)–(16c) for fixed $\mu = \mu_i$ and $h = 1$. We remark that exactly the same procedure can also be applied to get a numerical representation of the unstable eigenfunctions $\mathrm{v}_l, \ldots, \mathrm{v}_{n-1}$ and the associated unstable Floquet multipliers $\mu_l, \ldots, \mu_{n-1}$.

We remark that it may be advantageous to improve the numerical stabilty of the computation by continuing u_i as the solution of the equivalent boundary value problem

$$\dot{u}_i(t) = T_\gamma D_u f(u_\gamma(t), \lambda) u_i(t) + \ln|\mu_i|\, u_i(t), \tag{17a}$$

$$u_i(1) = \mathrm{sign}(\mu_i) u_i(0), \tag{17b}$$

$$\langle u_i(0), u_i(0) \rangle = 1; \tag{17c}$$

see [13] for details. Equations (17a)–(17c) were in fact used for the computations in section 4.3.

3.2. Step 1: Finding orbit segments up to Σ

As was mentioned before, the $(n-1)$-dimensional section Σ should be chosen such that it intersects the sought-after EtoP connection Q transversely. This can be achieved by choosing Σ such that the equilibrium p is on one side and the periodic orbit Γ on

the other side of Σ for all $\lambda \in \Lambda$. What is more, then any connecting orbit from p to Γ (that may exists for one or more $\lambda \in \Lambda$) intersects Σ, and the intersection is generically transverse. Indeed, the exact choice of Σ depends on the system under consideration; see the examples in section 4.

The first step of the method is now to find discretizations u^- and u^+ of the orbit segments Q^- and Q^+ from p to Σ and Γ to Σ, respectively. To this end, we fix the parameter λ at some value near λ^*. From section 3.1 we know (numerical representations of) the equilibrium p with its unstable eigendirections e_i^u, $i = 1, \ldots, k$, as well as the periodic orbit u_γ with the stable eigenfunctions u_i, $i = 1, \ldots, l-1$.

For u^- we consider the boundary value problem

$$\dot{u}^-(t) = T^- f(u^-(t), \lambda), \tag{18a}$$

$$\langle u^-(1) - p_\Sigma, n_\Sigma \rangle = \sigma^-, \tag{18b}$$

$$u^-(0) = p + \sum_{i=1}^{k} \varepsilon_i e_i^u. \tag{18c}$$

Here (18c) imposes a projection boundary condition on $u(0)$ at the equilibrium p. Namely, the parameters ε_i are the distances of $u^-(0)$ from p along the unstable eigendirections. Furthermore, the parameter σ^- measures the distance of the other endpoint $u^-(1)$ from Σ. For a fixed choice of small ε_i and starting from the trivial solution $u^- \equiv p + \sum_{i=1}^{k} \varepsilon_i e_i^u$ we continue (18a)–(18c) in the integration time $T^- > 0$ and in σ^-. The continuation is stopped when a zero of σ^- is detected, which means that we have found an initial orbit segment u^- starting near p in the unstable eigenspace and ending in Σ. We remark that it is convenient after the initial continuation up to Σ to implement the projection boundary condition in the form of a projection operation $L_u(p, \lambda)$ (represented by an $(n-k) \times n$ matrix) in combination with a phase condition; compare with [5, 11]. This means that we replace (18c) with

$$L_u(p, \lambda) u^-(0) = 0, \tag{19a}$$

$$\int_0^1 \langle \dot{\tilde{u}}^-(\tau), u^-(\tau) - \tilde{u}^-(\tau) \rangle d\tau = 0. \tag{19b}$$

The orbit segment u^+ is found similarly by considering the boundary value problem

$$\dot{u}^+(t) = T^+ f(u^+(t), \lambda), \tag{20a}$$

$$\langle u^+(0) - p_\Sigma, n_\Sigma \rangle = \sigma^+, \tag{20b}$$

$$u^+(1) = u_\gamma(0) + \sum_{i=1}^{l-1} \delta_i u_i(0). \tag{20c}$$

Here (20c) imposes a projection boundary condition on $u^+(1)$ at the point $u_\gamma(0)$ on the periodic orbit Γ. Namely, the parameters δ_i are the distances of $u^+(1)$ from $u_\gamma(0)$ along the stable Floquet directions $u_i(0)$, while σ^+ measures the distance of the other endpoint $u^+(0)$ from Σ. We again start with a fixed choice of small δ_i and the trivial solution $u^+ \equiv u_\gamma(0) + \sum_{i=1}^{l-1} \delta_i u_i(0)$ and continue (20a)–(20c) in the integration time $T^+ > 0$ and in σ^+. When $\sigma^+ = 0$ is detected we will have found an initial orbit segment u^- that starts in Σ and ends near Γ in the stable eigenspace. We remark that after the initial continuation in T it would be possible also to replace (20c) by a projection operator and an additional phase condition [3]. However, we find it more convenient to stick with the formulation (20c) in terms of the internal parameters δ_i,

which indeed implements a projection boundary condition at Γ since the δ_i are free to vary during the continuation.

3.3. Step 2: Setting up the Lin space

The Lin space Z is a d-dimensional subspace of the space Y (from the definition (6) of Σ) that satisfies (12). Once Z has been chosen we need to ensure that $u^+(0) - u^-(1) \in Z$. Indeed there are many possibilities for choosing Z, and we discuss here a few convenient choices as used in section 4.

We first consider the case that $\dim Z = 1$ when we also talk of Z as the Lin direction. Then a straightforward option is to define $Z = \mathrm{span}\{u^+(0) - u^-(1)\}$, which generically satisfies (12). (Note that here $\lambda \neq \lambda^*$.) Another option is to consider the curves that are traced out by $u^-(1)$ and $u^+(0)$ (still for fixed λ) when one continues the orbit segments u^- and u^+ in (a suitable combination of) (ε_i, T^-) and (δ_i, T^+), respectively. The Lin direction Z can then be chosen as that through the two points of these families that are closest to each other. In this way, the initial Lin gap along Z is as small as possible; see section 4.1 and section 4.2.

More generally, one can choose Z as any d-dimensional subspace. A convenient choice used in section 4.3 is that of a d-dimensional hyperplane parallel to some of the coordinate axes. A continuation of (20a)–(20c) for fixed $\sigma^+ = 0$ in T^+ and (a suitable combination of) δ_i can then be used to ensure that $u^+(0) - u^-(1) \in Z$.

Finally, we select an orthonormal basis z_i, $i = 1, \ldots, d$ of Z. This allows us to initialize the (signed) Lin gaps η_i, $i = 1, \ldots, d$, such that

$$u^+(0) - u^-(1) = \sum_{i=1}^{d} \eta_i z_i \,, \tag{21}$$

in accordance with theorem 2.1.

3.4. Step 3: Closing the Lin gaps

The orbit segments u^- and u^+ that we have obtained after steps 1 and 2 above, are the discretizations of the unique orbit segments Q^- and Q^+ of theorem 2.1. Namely, u^- and u^+ are isolated orbit segments that satisfy projection boundary conditions near p and Γ and whose difference in Σ lies in the Lin space Z. They represent a solution of a large λ-dependent boundary value problem, as formulated step-by-step in the above sections, that also involves the equilibrium, the periodic orbit and their linear eigendirections. It can be formulated as

$$\begin{aligned}
f(p,\lambda) &= 0, && (22a)\\
\dot{u}_\gamma(t) &= T_\gamma f(u_\gamma(t),\lambda), && (22b)\\
u_\gamma(0) &= u_\gamma(1), && (22c)\\
\int_0^1 \left\langle \dot{\tilde{u}}_\gamma(\tau), u_\gamma(\tau) \right\rangle d\tau &= 0, && (22d)\\
\dot{u}_i(t) &= T_\gamma D_u f(u_\gamma(t),\lambda) u_i(t), && (22e)\\
u_i(1) &= \mu_i u_i(0), && (22f)\\
\langle u_i(0), u_i(0) \rangle &= 1, \qquad (i = 1, \ldots, l-1) && (22g)\\
\dot{u}^-(t) &= T^- f(u^-(t),\lambda), && (22h)
\end{aligned}$$

$$\langle u^-(1) - p_\Sigma, n_\Sigma \rangle = 0, \tag{22i}$$

$$L_u(p,\lambda)u^-(0) = 0, \tag{22j}$$

$$\int_0^1 \langle \dot{\tilde{u}}^-(\tau), u^-(\tau) - \tilde{u}^-(\tau)\rangle d\tau = 0, \tag{22k}$$

$$\dot{u}^+(t) = T^+ f(u^+(t),\lambda), \tag{22l}$$

$$u^+(1) = u_\gamma(0) + \sum_{i=1}^{l-1} \delta_i u_i(0), \tag{22m}$$

$$(u^+(0) - u^-(1)) = \sum_{i=1}^{d} \eta_i z_i. \tag{22n}$$

Equations (22*b*), (22*e*), (22*h*) and (22*l*) form a system of $N = (3n+(l-1)n)$ equation. (Note that equation (22*a*) for the equilibrium is well-posed in itself and, hence, is not included in this count.) Similarly, we can combine the boundary conditions and integral constraints (22*c*), (22*d*), (22*f*), (22*g*), (22*i*), (22*j*), (22*k*), (22*m*) and (22*n*) into a system of $B = (4n + (l-1)n + l - k + 2)$ constraints. Thus for every value of the system parameter $\lambda \in \Lambda$ the $B - N = n + l - k + 2$ internal parameters T_γ, T^+, T^-, $\delta_1, \ldots, \delta_{l-1}$, $\mu_1, \ldots, \mu_{l-1}$, $\eta_1, \ldots, \eta_d$ are uniquely determined, meaning that system (22*a*)–(22*n*) is well posed [11].

The strategy is now to free the system parameter $\lambda = (\lambda_1, \ldots, \lambda_m)$ in a systematic way to close the Lin gaps $\eta_1, \ldots, \eta_d$ one by one by performing well-defined continuation runs; compare with [31]. Assuming that at the start $\eta_i \neq 0$ for all $i = 1, \ldots, d$ to begin with, we continue (22*a*)–(22*n*) in the first run in λ_1, T_γ, T^+, T^-, $\delta_1, \ldots, \delta_{l-1}$, $\mu_1, \ldots, \mu_{l-1}$, $\eta_1, \ldots, \eta_d$ until η_1 is zero. We then fix $\eta_1 = 0$ and replace the parameter η_1 by a second family parameter λ_2. That is, in the second run we continue (22*a*)–(22*n*) in λ_1, λ_2, T_γ, T^+, T^-, $\delta_1, \ldots, \delta_{l-1}$, $\mu_1, \ldots, \mu_{l-1}$, $\eta_2, \ldots, \eta_d$ until, without loss of generality, $\eta_2 = 0$. Proceeding in this manner, in the j-th run the continuation parameters are $\lambda_1, \ldots, \lambda_j$, T_γ, T^+, T^-, $\delta_1, \ldots, \delta_{l-1}$, $\mu_1, \ldots, \mu_{l-1}$, $\eta_j, \ldots, \eta_d$, while $\eta_1 = \ldots = \eta_{j-1} = 0$.

After d consecutive continuation runs all Lin gaps η_i are zero and we have $\lambda = \lambda^*$. The concatenation of the orbit segments u^- and u^+, which satisfy $u^-(1) = u^+(0)$, is the sought discretization of the connecting orbit Q of (1). It can be continued in further system parameters λ_i for $i > d$ while keeping $\eta_1 = \ldots = \eta_d = 0$.

We remark that it is possible that there exist several solutions where all Lin gaps are closed. Each such solution corresponds to a different EtoP connection at an isolated point in $(\lambda_1, \ldots, \lambda_d)$-space. On the other hand, if it is not possible to find a solution where all Lin gaps are closed then the sought-after EtoP connection Q does not exist in the parameter region Λ.

3.5. Computation of related objects

A codimension-d EtoP connection Q typically implies the existence of other orbits involved in the bifurcation diagram that are related to Q. Therefore, the continuation of Q provides a starting point for unravelling a bifurcation diagram. We now discuss some related objects and how they can be found and continued.

First of all, with the codimension-d EtoP connection Q one often finds a second connection R from Γ back to p. This second EtoP connection is generically of codimension zero. It can be found by performing steps 1 and 2 above to find a

(generic) intersection point of $W^u(\Gamma) \cap \Sigma$ and $W^s(p) \cap \Sigma$ for some initial λ; in this continuation $\dim Z = 0$, so that restricting the difference of $u^-(1)$ and $u^+(0)$ to Z means achieving $u^-(1) - u^+(0) = 0$ Note that in the setup in section 3.2 and section 3.3 time T is reversed in (13). The resulting connecting orbit can then be continued in λ. However, in low-dimensional examples it is generally easier to obtain a codimension-zero EtoP connection R by a so-called homotopy method; see [13, 17]. Namely one starts in the linear unstable eigenspace near the periodic orbit Γ and continues in the integration time T (effectively performing shooting) until the linear stable eigenspace of p is reached. The distance to the equilibrium p can then be reduced in a further continuation. The codimension-zero EtoP connection in sections 4.1 and 4.2 were found in this way. Specifically, the connecting orbit R is represented by an orbit segment u_r and can then be continued, together with p, Γ and their linear eigenspaces, as the solution of the boundary value problem

$$\dot{u}_r(t) = Tf(u_r(t), \lambda), \tag{23a}$$

$$u_r(0) = u_\gamma(0) + \sum_{i=l}^{n-1} \delta_i u_i(0), \tag{23b}$$

$$L_s(p, \lambda) u_r(1) = 0, \tag{23c}$$

$$\int_0^T \left\langle \dot{\tilde{u}}_r(\tau), u_r(\tau) - \tilde{u}_r(\tau) \right\rangle d\tau = 0. \tag{23d}$$

Here we use the unstable Floquet directions u_i, $i = l, \ldots, n-1$ for the approximation of $W^u(\Gamma)$, while the projection boundary condition near p is given by the projection $L_s(p, \lambda)$ onto the linear stable eigenspace of p. The boundary value problem (23*a*)–(23*d*) is well posed if $W^u(\Gamma)$ and $W^s(p)$ intersect transversely along an isolated orbit, which is R. Note that generically this is always the case when the original EtoP connection Q is of codimension one. In this situation u_r can be continued in the parameter λ as a solution of (23*a*)–(23*d*). We only remark that if $W^u(\Gamma)$ and $W^s(p)$ intersect along a manifold of dimension larger than one, additional conditions are needed to select a single connecting orbit R within the intersection.

Together the codimension-d EtoP connection Q and the codimension-zero EtoP connection R form an EtoP heteroclinic cycle between p and Γ, which can be continued in parameters. Theory predicts that other types of global orbits exists near such an EtoP heteroclinic cycle; see [6, 22, 33]. Start data for these expected global objects can be obtained by concatenating the orbit segments representing Q and R in appropriate ways. For example, a codimension-d homoclinic orbit connecting p back to itself can be constructed in good approximation as the concatenation of u^-, u^+ and u_r, provided $u_r(0)$ and $u^+(1)$ are sufficiently close together. After an initial Newton step, the homoclinic orbit can readily be continued with the HomCont extension of Auto; see section 4.2 where we investigate the interaction of this kind of homoclinic orbit with the EtoP heteroclinic cycle. Another type of orbit that must be expected near the EtoP heteroclinic cycle is a homoclinic orbit to Γ, which is generically of codimension zero. Again, we can concatenate orbit segments as start data for the discretized homoclinic orbit u_h, which (for each λ) satisfies the boundary value problem

$$\dot{u}_h(t) = T_h f(u_h(t), \lambda), \tag{24a}$$

$$u_h(0) = u_\gamma(0) + \sum_{i=l}^{n-1} \delta_i u_i(0), \tag{24b}$$

$$u_h(1) = u_\gamma(0) + \sum_{i=1}^{l-1} \delta_i u_i(0). \tag{24c}$$

Note that (24*a*)–(24*a*) is well posed, as it consist of $2n$ boundary conditions that determine u_h and the n additional parameters T_h, $\delta_1, \ldots, \delta_{n-1}$.

More generally, the boundary value problems in section 3 provide a 'toolkit' for the continuation of connecting orbits that we are interested in. As is demonstrated in the next section, the construction of the initial codimension-d EtoP connection with Lin's method serves as a stepping stone for the continuation of many associated connecting orbits.

4. Demonstration of the method

We now demonstrate our method for finding and continuing EtoP connections and related EtoP heteroclinic cycles with three examples. Namely, we consider the well-known Lorenz system [29], a three-dimensional vector-field model of a saddle-node Hopf bifurcation with global reinjection [22], and a four-dimensional coupled Duffing system [27]. All computations are performed with the numerical continuation package AUTO2000/AUTO07P [15, 16], which uses pseudo-arclength continuation and orthogonal collocation to solve the boundary value problems that arise; see [11] for more details. The size of the overall boundary value problems is given by the number of objects that are continued simultaneously, which typically include the equilibrium p, the periodic orbit Γ together with its stable and its unstable eigenfunctions, and the two orbit segments Q^- and Q^+ up to the specified section Σ. Throughout we use polynomials of degree `NCOL` $= 4$ in each collocation interval and, depending on the complexity of the orbit, between `NTST` $= 200$ and `NTST` $= 1000$ collocation intervals. (Note that this means that Γ, Q^- and Q^+ are all represented over the same mesh as given by `NCOL` and `NTST`).

4.1. Codimension-one EtoP heteroclinic cycle in the Lorenz system

In the 1960's Lorenz derived the much simplified model of atmospheric convection [29] given by the three-dimensional vector field

$$\begin{cases} \dot{x} &= \sigma(y - x), \\ \dot{y} &= \varrho x - y - xz, \\ \dot{z} &= xy - \beta z. \end{cases} \tag{25}$$

For the classical choice of parameters given by $\beta = \frac{8}{3}$, $\sigma = 10.0$ and $\varrho = 28$ found the now well-known butterfly or Lorenz attractor, which is one of the best known examples of chaotic dynamics (i.e. sensitive dependence on the initial condition).

When the parameter ϱ is allowed to vary, there is a transition from simple to chaotic dynamics. It involves a homoclinic bifurcation at $\varrho_{\rm hom} \approx 13.9265$ where there is a pair of homoclinic orbits to the origin $\mathbf{0}$ that are each other's images under the symmetry transformation

$$(x, y, z) \mapsto (-x, -y, z)$$

of (25). For $\varrho_{\rm het} \approx 24.0579$ there exists a symmetric pair of EtoP connections between $\mathbf{0}$ and periodic orbits Γ^+ and Γ^-; see [14, 36] for more details. Here we find and follow in parameters (one of) these EtoP connections and the associated EtoP heteroclinic

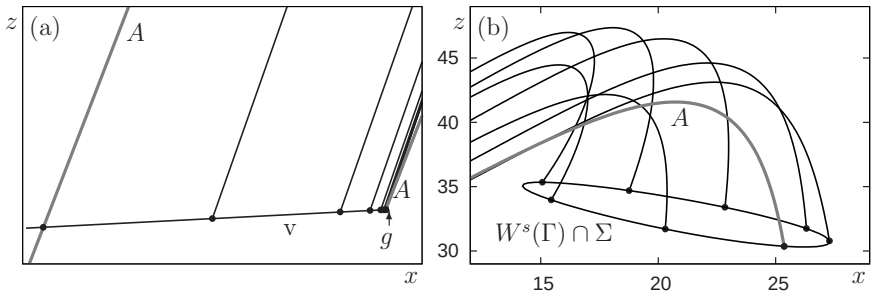

Figure 2. Orbit segments during the computation of $W^s(\Gamma)$ up to the section Σ in the Lorenz system (25) for $\sigma = 10.0$, $\varrho = 28.0$, and $\varrho = 24.5$. Panel (a) shows the end points of different orbit segments along the stable Floquet direction v; the orbit A bounds a fundamental domain. The length of the fundamental domain is 1.55752×10^{-5}. Panel (b) shows how the other end points trace out $W^s(\Gamma) \cap \Sigma$.

cycle. The origin $\mathbf{0}$ is a saddle-point for $\varrho > 1$ with a one-dimensional unstable manifold and a two-dimensional stable manifold, as determined by the eigenvalues

$$-\beta \quad \text{and} \quad -\frac{1}{2}(\sigma+1) \pm \frac{1}{2}\sqrt{(\sigma+1)^2 + 4\sigma(\varrho-1)}.$$

The periodic orbit Γ can been found by continuation from a Hopf bifurcation at $\varrho_H \approx 24.7368$ of the non-zero equilibria secondary equilibria

$$p^{\pm} = (\pm\sqrt{\beta(\varrho-1)}, \pm\sqrt{\beta(\varrho-1)}, \varrho-1).$$

Indeed Γ is of saddle type and its stable eigenspace can be computed as described in section 3. Due to the symmetry it is sufficient to consider only the connection from $\mathbf{0}$ to $\Gamma = \Gamma^-$ which lies in the one-dimensional unstable manifold of $\mathbf{0}$ and the two-dimensional stable manifold of Γ.

4.1.1. Finding the codimension-one EtoP connection We define the section Σ by specifying the point $p_\Sigma \in W^u(\mathbf{0})$ (for $\varrho = 24.0579 \approx \varrho_{\text{het}}$ and β, σ at their classical values) that satisfies

$$\text{dist}(p_\Sigma, \mathbf{0}) \approx \text{dist}(p_\Sigma, \Gamma).$$

which gives

$$p_\Sigma = \begin{pmatrix} 17.2877 \\ 21.4376 \\ 31.7958 \end{pmatrix}.$$

Further, the normal vector n_Σ of Σ is defined as the direction of the flow at p_Σ.

To start, we choose $\varrho = 24.5$ as an initial parameter value reasonably close to ϱ_{het}. The first step (cf. section 3.2) consists of a computation of the one-dimensional manifold $W^u(\mathbf{0})$ by continuation in the direction of positive time T^- from $\mathbf{0}$, subject to boundary condition (18c), until the section Σ is reached. Similarly, we choose a point $g \in \Gamma$, $g = (-10.0437, -9.95751, 25.7945)$, and consider the corresponding fixed stable Floquet vector v for the formulation of boundary condition (20c). We then continue in the direction of time T^+ until Σ is reached. A further continuation in the distance δ along v yields the one-dimensional intersection curve $W^s(\Gamma) \cap \Sigma$.

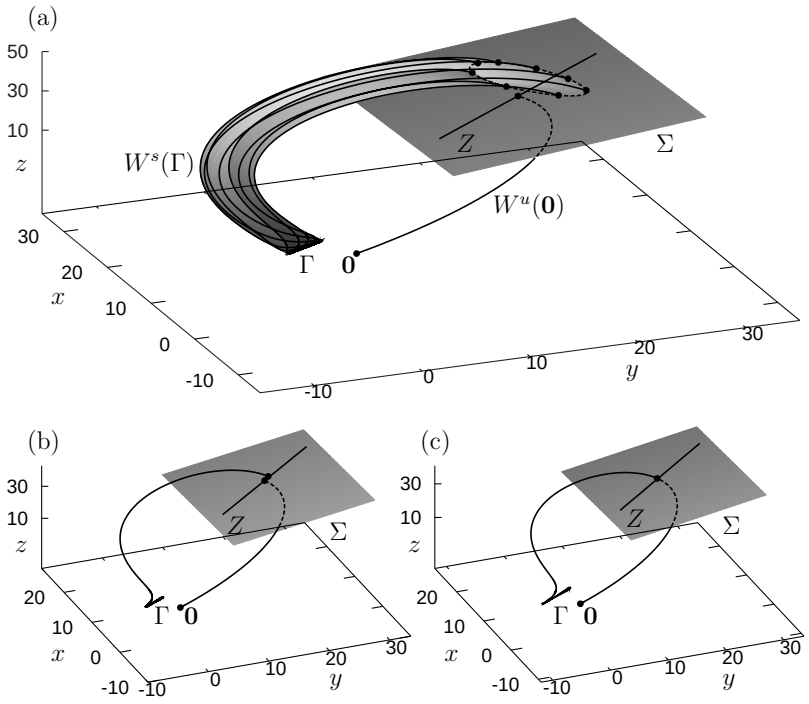

Figure 3. The manifolds $W^u(\mathbf{0})$ and $W^s(\Gamma)$ of (25) computed up to the section Σ for $\varrho = 24.5$ with a Lin gap along Z of $\eta = 1.39437$ (a); panel (b) only shows the two orbit segments up to Z. For $\varrho = 24.0579$ where $\eta = 0$ was detected the two orbit segments connect in Σ (c). Throughout, $\beta = 8/3$ and $\sigma = 10.0$.

Figure 2 (a) shows the end points $u^+(1)$ of orbit segments on v near the chosen fixed base point $g \in \Gamma$. The orbit denoted by A intersects the Floquet vector v twice and thus bounds a fundamental domain. While $u^+(1)$ on v cover the fundamental domain on v, the other end point $u^+(0)$ traces out the intersection curve $W^s(\Gamma) \cap \Sigma$. As figure 2(b) shows, this curve is a smooth closed curve in Σ. Figure 3(a) shows the computed parts of $W^u(\mathbf{0})$ and $W^s(\Gamma)$ in (x, y, z)-space, where the section Σ is the gray plane. Notice that $W^s(\Gamma)$ is a topological cylinder that is represented well by the family of orbit segments parametrized by δ.

Next we need to make a suitable choice for the one-dimensional Lin direction Z; cf. section 3.3. As was mentioned before, a good choice is to define Z as the derection given by $W^u(\mathbf{0}) \cap \Sigma$ and the point on $W^s(\Gamma) \cap \Sigma$ that lies closest to it. Then the initial Lin gap along Z is as small as possible. The respective orbit segments of $W^u(\mathbf{0})$ and $W^s(\Gamma)$ are shown in figure 3(b); the initial gap size is $\eta = 1.39437$.

To close the Lin gap η and find the codimension-one EtoP connection we continue in the parameters T^-, T^+, η and ϱ; cf. section 3.4 and (22a)–(22n). For $\varrho = 24.0579$ a zero of η is detected; figure 3(c) depicts the EtoP connection from $\mathbf{0}$ to Γ. Note that

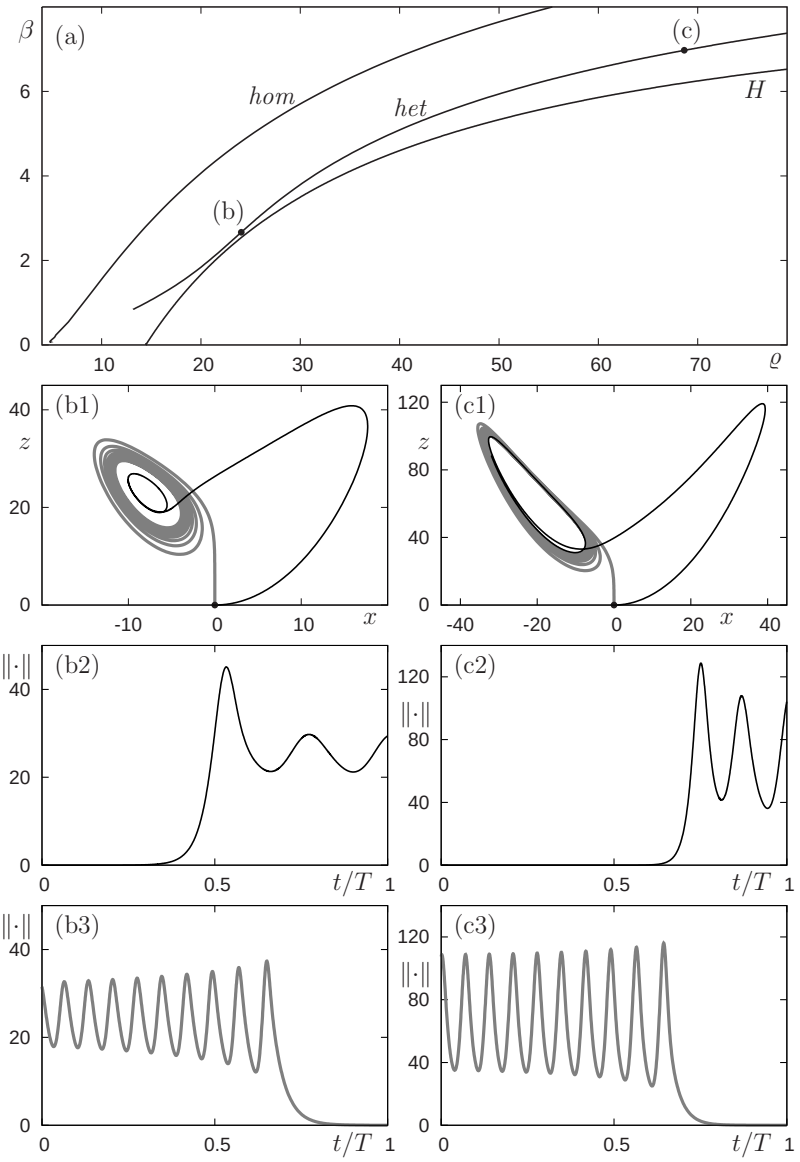

Figure 4. Panel (a) shows the curve *het* of EtoP connections from $\mathbf{0}$ to Γ, the curve *hom* of the homoclinic connection to $\mathbf{0}$ and the curve H of Hopf bifurcation in the (ϱ, β)-plane of (25). Panels (b) and (c) show the computed EtoP heteroclinic cycle for the two selected parameter values $(\varrho, \beta) = (24.0579, 2.66667)$ and $(\varrho, \beta) = (68.6494, 6.97370)$, respectively. Specifically, panels (b1) and (c1) show the projection onto the (x, z)-plane; panels (b2) and (c2) show the norm of the codimension-one connection from $\mathbf{0}$ to Γ; and panels (b3) and (c3) show the norm of the codimension-zero connection from Γ back to $\mathbf{0}$.

this value agrees within the computational accuracy of $\varrho_{\rm het}$ found in [14].

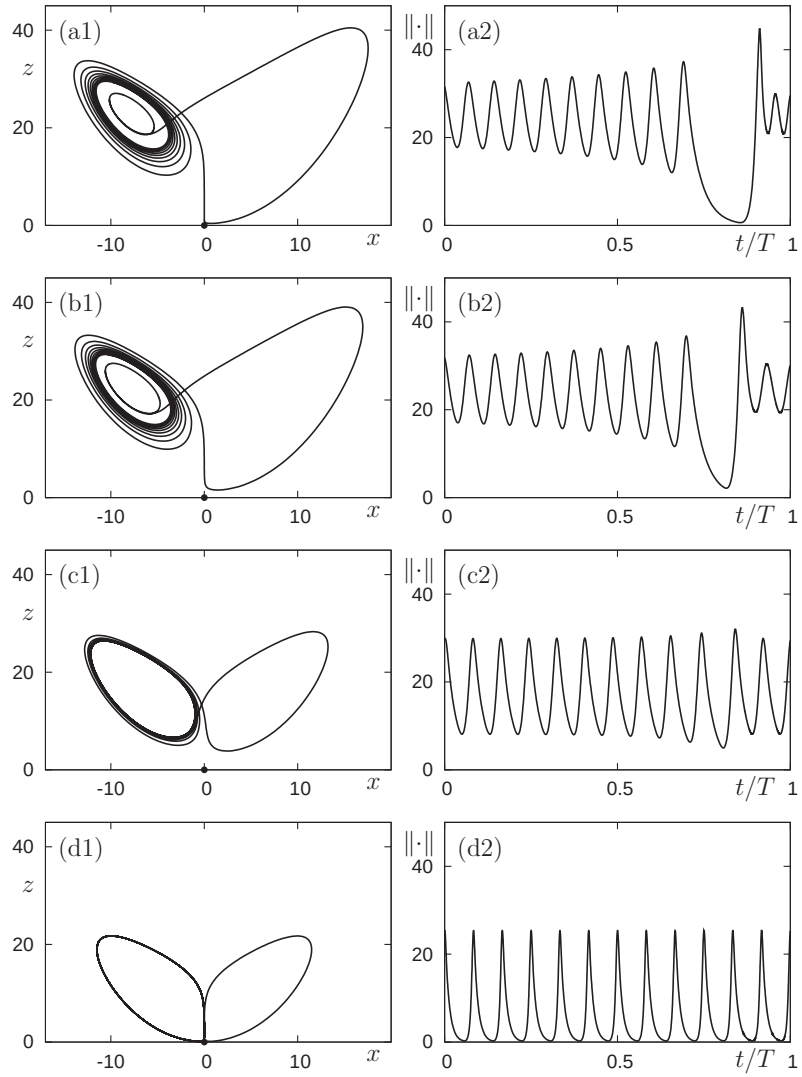

Figure 5. The codimension-zero homoclinic orbit to Γ of (25) for $\beta = 8/3$ and $\sigma = 10.0$ in dependence on ϱ. Shown are the projection onto the (x, z)-plane (left column) and the norm of the approximating orbit segment (right column) for $\varrho = 23.9666$ (a), $\varrho = 23.5575$ (b), $\varrho = 18.6310$ (c), and $\varrho = 13.9828$ (d).

These computations show that our method is indeed able to find a first solution for the continuation of the codimension-one EtoP connection. Namely, the two orbit segments can now be continued in system parameters while keeping $\eta = 0$ fixed. As was explained in section 3.5, we find the codimension-zero connection from Γ back to p as the solution of the boundary value problem defined by $(23a)$–$(23d)$ by starting from a suitable initial orbit segment.

4.1.2. Continuation of the EtoP cycle The entire codimension-one EtoP heteroclinc cycle can be continued in two system parameters. Figure 4(a) shows the resulting codimension-one bifuraction curve *het* and the bifurcation curve *hom* of the homoclinic explosion in the (ϱ, β)-plane; also shown is the Hopf bifurcation curve H. Panels (b1) and (c1) show two examples of the corresponding EtoP heteroclinic cycle in projection onto the (x, z)-plane, which consists of the codimension-one connection from $\mathbf{0}$ to Γ (black curve) and the codimension-zero connection from Γ back to $\mathbf{0}$ (gray curve). The two respective time traces of the norm $\|\cdot\|$ of the approximating orbit segments (subject to projection boundary conditions) are shown in figure 4 (b2)/(c2) and (b3)/(c3), respectively.

When computing the codimension-one connection for decreasing ϱ towards the homoclinic bifurcation *hom* we encountered some difficulties with the calculation of the two Floquet multipliers of Γ, which could only be determined reliably for $\varrho > 13.1703$. This problem might be solved by employing a more accurate method for determining Floquet multipliers, such as that in [30], but this is beyond the scope of this paper. The codimension-zero connection from Γ back to $\mathbf{0}$, on the other hand, could be computed throughout, that is, the intersection of $W^u(\Gamma)$ and $W^s(\mathbf{0})$ remains transverse; an example where this intersection becomes tangential is presented in section 4.2.

To demonstrate that the EtoP heteroclinic cycle can be used as a starting solution for the numerical continuation of other types of orbits, we compute the codimension-zero homoclinic orbit to Γ; for $\beta = 8/3$ and $\sigma = 10.0$ it exists for $\varrho \in (\varrho_{\rm hom}, \varrho_{\rm het}) \approx (13.9265, 24.0579)$. To obtain a first homoclinic orbit we concatenate the two separate heteroclinic conncetions near the fixed point p as a seed for a Newton solve of the boundary value problem defined by $(24a)$–$(24c)$. The resulting approximation (subject to projection boundary conditions $(24b)$,$(24c)$ at both ends) of the homoclinic orbit to Γ can then be continued (together with Γ and its Floquet bundles) in a system parameter. Figure 5 shows the homoclinic orbits to Γ for different values of ϱ. Panel (a) is for ϱ close to $\varrho_{\rm het}$ and the homoclinic orbit passes very close to the origin $\mathbf{0}$ after a single excursion to the right, that is, into the region of positive x. As ϱ is decreased, the orbit deforms but maintains its overall structure with a single excursion to the right; see figure 5(b) and (c). At the same time the periodic orbit $\Gamma = \Gamma^-$ (and its counterpart Γ^+) move toward $\mathbf{0}$ and the homoclinic orbit to Γ approaches the union of the two symmetrically related homoclinic orbits to $\mathbf{0}$ as the homoclinic explosion point at $\varrho_{\rm hom} \approx 13.9265$ is approached; see figure 5(d). This shows that the homoclinic orbit to Γ considered here is one of the infinitely many connecting orbits that are born in the homoclinic explosion; see also [14].

4.2. Global reinjection orbits near a saddle-node Hopf bifurcation

In this section we compute connecting orbits in a three-dimensional model vector field that was introduced in [22] to describe the dynamics near a saddle-node Hopf bifurcation in the presence of a global reinjection mechanism. This type of dynamics with reinjection can be found, for example, in laser systems [24, 39, 42], in dynamo theory [2] and, more generally, near weak resonances [38, chapter 4.3.2]. The vector-

field model can be written in the form

$$\left\{\begin{array}{rcl} \dot{x} &=& \nu_1 x - \omega y - (\alpha x - \beta y)\sin\varphi - (x^2+y^2)x \\ & & \qquad +d(2\cos\varphi+\nu_2)^2, \\ \dot{y} &=& \nu_1 y + \omega x - (\alpha y + \beta x)\sin\varphi - (x^2+y^2)y \\ & & \qquad +f(2\cos\varphi+\nu_2)^2, \\ \dot{\varphi} &=& \nu_2 + s(x^2+y^2) + 2\cos\varphi + c(x^2+y^2)^2, \end{array}\right. \tag{26}$$

where ν_1 and ν_2 are the unfolding parameters of the saddle-node Hopf bifurcation. The parameters ω, α, β, s, c, d and f determine the type of unfolding and we keep them fixed throughout at

$$\omega = 1.0,\ \alpha = -1.0,\ \beta = 0,\ s = -1.0,\ c = 0,\ d = 0.01,\ f = \pi d.$$

This choice corresponds to the unfolding of type A that was studied in [22], where more details can be found. The variable φ is 2π-periodic and global reinjection is realized by trajectories that connect a neighbourhood of a saddle-node Hopf point with one of its symmetric copies. When representing trajectories it is convenient to show them in (u, v, w)-space as given by the transformation

$$\left\{\begin{array}{rcl} u &=& (R+x)\cos\varphi, \\ v &=& (R+x)\sin\varphi, \\ w &=& y, \end{array}\right. \tag{27}$$

where a global reinjection corresponds to a large excursion near the circle $\mathbb{S}^1 = \{x = y = 0\}$. Note that this circle is not invariant because $d \neq 0$ and $f \neq 0$ (where rational ratios are avoided). We fix the radius $R = 2$, which is large enough in light of the x-amplitudes of observed solutions.

As was shown in [22], system (26) features a complicated structure of homoclinic orbits of equilibria that involve one or more global reinjections. Furthermore, some of the corresponding homoclinic bifurcation curves accumulate on curve segments, while the homoclinic orbit itself accumulates on a periodic orbit of saddle type. This global bifurcation phenomenon was studied theoretically in [33] and (26) provides the first concrete example. Here we demonstrate how the bifurcation diagrams from [22] can be completed with our method.

4.2.1. Codimension-one EtoP heteroclinic cycle Our starting point is the two-parameter bifurcation diagram of system (26) given in figure 6, which only shows the bifurcation curves that were presented in [22]. Two saddle-node Hopf points $SNH^{\pm}$ on two lines S_0 of saddle-node bifurcations are connected by a Hopf bifurcation curve H. the curve S_l of saddle-node bifurcations of periodic orbits emerges from a degenerate Hopf point DH. The most interesting object is the curve h_b^1 of homoclinic orbits that connect the saddle-focus $b = (0, 0, \arccos(\nu_2/2))$ back to itself after a single global reinjection. As can be seen in the enlargement panels (b) and (c), h_b^1 emerges from a non-central saddle-node homoclinic point NS, crosses S_l and then accumulates on a curve segment in the (ν_1, ν_2)-plane. As was mentioned, this accumulation process implies the existence of a EtoP heteroclinic cycle connecting the saddle point b with a periodic orbit Γ of saddle type. Note that we have $\dim W^u(\Gamma) = 2$ and $\dim W^s(b) = 1$, thus we reverse time in the formulation of the boundary value problems in section 3.

To find the EtoP heteroclinic connection between the equilibrium b and the periodic orbit Γ, we choose the section $\Sigma = \{v = 0\}$ and start from a point in parameter space close to the segment of accumulation of h_1^b; compare with figure 6(c). Specifically, we fix $\nu_2 = -1.46$ and start the computation from $\nu_1 = 0.706987$. First

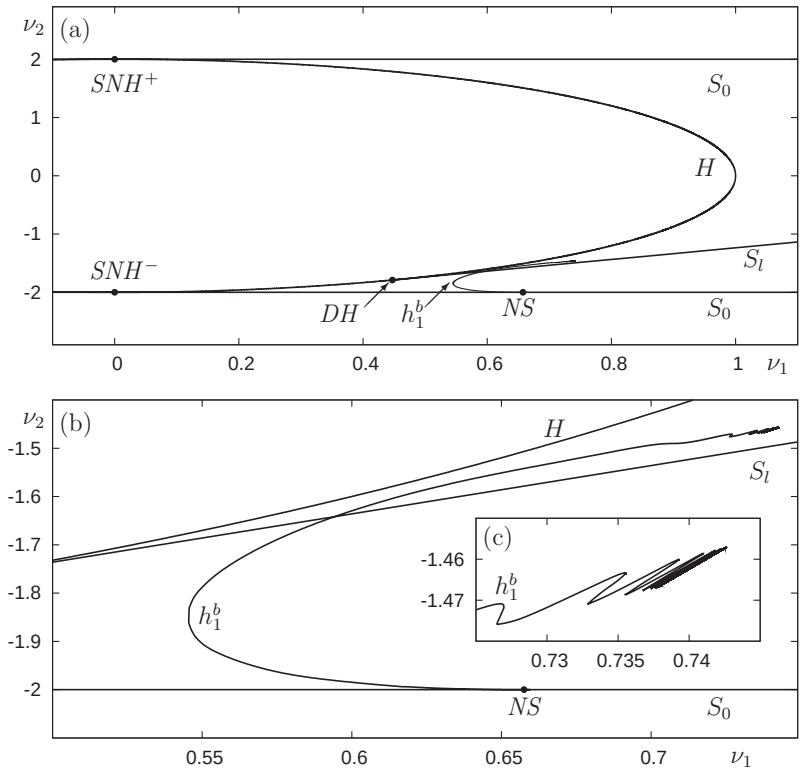

Figure 6. Bifurcation diagram in the (ν_1, ν_2)-plane of (26) consisting of two saddle-node bifurcation curves S_0 and a Hopf bifurcation curve H that meet at two saddle-node Hopf points $SNH^{\pm}$, a curve S_l of saddle-node bifurcations of periodic orbits, and a homoclinic bifurcation curve h_b^1. Panel (a) shows an overview, and panels (b) and (c) are successive enlargements of the curve h_b^1.

we compute $W^s(b)$ by continuation in T^+ until the section Σ is reached; cf. section 3.2 and (18*a*)–(18*c*). We then fix a vector $\mathrm{v}(g)$ of the unstable bundle of Γ at a chosen point $g = (0.226499, -0.226726, 5.69218)$, to specify the boundary condition (20*c*) and continue in the direction of time T^- until Σ is reached. Continuation in the distance δ along v over a fundamental domain is then used to compute the curve $W^u(\Gamma) \cap \Sigma$; figure 7 shows that it is again a smooth closed curve in Σ. Figure 8(a) shows $W^s(b)$ and $W^u(\Gamma)$ in (u, v, w)-space as computed up to the section Σ (gray plane). $W^u(\Gamma)$ is a topological cylinder and well represented by a suitable selection of orbit segments as parametrised by δ.

As in section 4.1, we choose the Lin direction Z as the line through $W^u(b) \cap \Sigma$ and the point on $W^s(\Gamma) \cap \Sigma$ closest to it; cf. section 3.3. The respective orbit segments of $W^u(b)$ and $W^s(\Gamma)$ that end in Z are shown in figure 8(b), where the gap size is $\eta = 0.1$. By continuation in T^-, T^+, η and ν_1 the Lin gap is closed; cf. section 3.4 and (22*a*)–(22*n*). Namely, a zero of η is detected at $\nu_1 = 0.741189$; the corresponding connecting orbit is shown in figure 8(c).

The codimension-one connecting orbit from Γ to b can now be continued in the parameters ν_1 and ν_2 while keeping the gap closed. This yields the curve c_b that

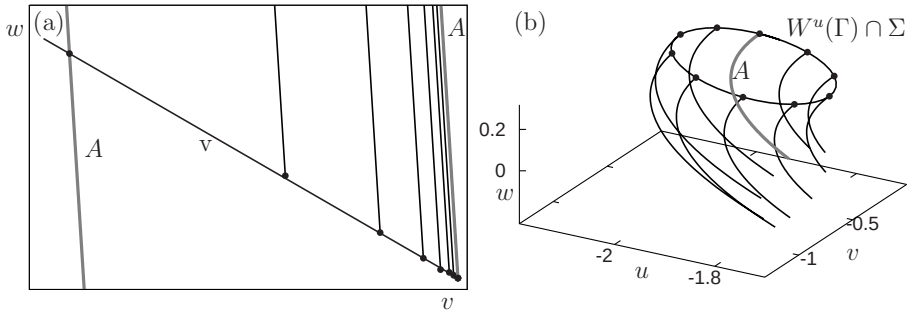

Figure 7. Orbit segments during the computation of $W^u(\Gamma)$ of (26) up to the section Σ. Panel (a) shows the end points of different orbit segments along the stable Floquet direction v; the orbit A bounds a fundamental domain; the length of the fundamental domain is $1.42163 \cdot 10^{-8}$. Panel (b) shows how the other end points trace out $W^u(\Gamma) \cap \Sigma$.

is shown as part of the bifurcation diagram in figure 9. One end point of c_b is the point SC_1 on the curve S_l of saddle-node bifurcations of the periodic orbit, where Γ disappears. The other end point of c_b is the point HSH_1 on the curve H of Hopf bifurcation where Γ shrinks down to the equilibrium a. At HSH_1 a codimension-two connection between b and a exists, that is, the branches of the one-dimensional manifolds $W^u(a)$ and $W^s(b)$ coincide. This codimension-two point is one of the possible 'heteroclinic equivalents' of a Shilnikov-Hopf bifurcation; see [20]. A segment of the curve c_b indeed appears to be the limit of the oscillating curve h_1^b; see figure 9(c).

In system (26) the codimension-zero EtoP connection from b back to Γ exists only in a certain region of the (ν_1, ν_2)-plane, namely near the accumulation of the curve h_1^b on c_b. This structurally stable intersection of the two-dimensional manifolds $W^u(b)$ and $W^s(\Gamma)$ can be computed as was explained in section 3.5 using the boundary value problem (23*a*)–(23*d*). The boundary of its region of existence is formed by curves t_b where $W^u(b)$ and $W^s(\Gamma)$ become tangent. The curves t_b can be continued as folds of the respective codimension-zero EtoP connection; they are shown in figure 9(b) and (c) as part of the bifurcation diagram in the (ν_1, ν_2)-plane. For increasing ν_1 the curves t_b can be continued up a point (not shown) on S_l, where the periodic orbit Γ disappears in a saddle-node bifurcation. When ν_1 is decreased, the curves t_b cross the Hopf curve H where Γ disappears in the equilibrium a. As a consequence, the codimension-zero EtoP connection changes its nature along the curve segment HSH_2 on H; see figure 9(b). Namely, beyond HSH_2 (for smaller ν_1) there is now a codimension-zero heteroclinic connection between the two-dimensional manifolds $W^u(b)$ and $W^s(a)$. Hence, beyond H the curves t_b correspond to tangencies of $W^u(b)$ and $W^s(a)$. Such tangencies, that is, the curves t_b, can be continued to the point SNH^-; see figure 9(a). We remark that the heteroclinic bifurcation at HSH_2 can be described as another type of 'heteroclinic equivalent' of a Shilnikov-Hopf bifurcation; see [20].

We observe in figure 9(b) and (c) that the curves t_b appear to bound the accumulation process of the curve h_1^b on c_b. After it enters the region in the (ν_1, ν_2)-

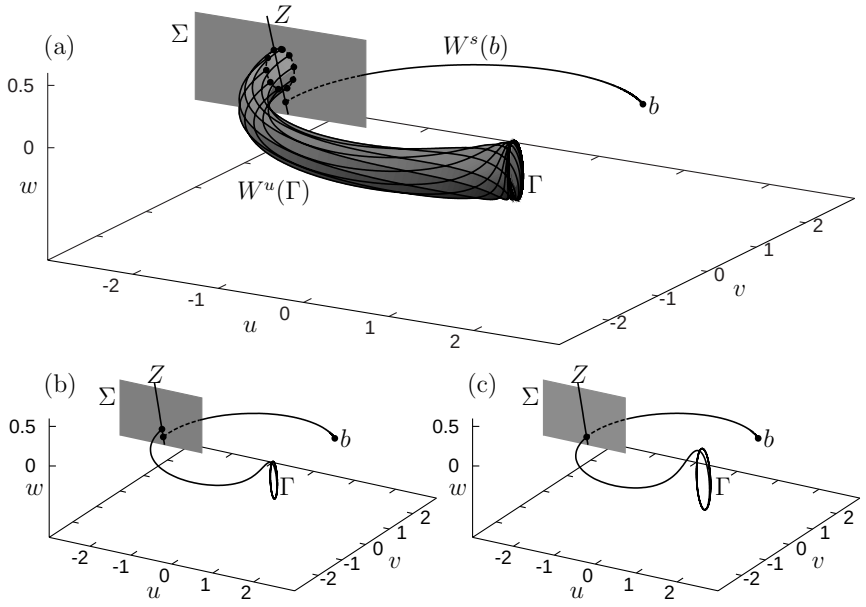

Figure 8. The manifolds $W^s(b)$ and $W^u(\Gamma)$ of (26) computed up to the section Σ for $\nu_1 = 0.706987$ with a Lin gap along Z of $\eta = 0.1$ (a); panel (b) only shows the two orbit segments up to Z. For $\nu_1 = 0.741189$ where $\eta = 0$ was detected the two orbit segments connect in Σ (c). Throughout, $\nu_2 = -1.46$.

plane that is bounded by t_b, the curve h_1^b oscillates between these bounds; see figure 9(c). Figure 10 shows homoclinic orbits in parameter space and as w-time plots for the maxima (w.r.t. ν_1) that are indicated in figure 9(c). From maximum to maximum of h_1^b the corresponding homoclinic orbit from b back to itself makes one more turn around the periodic orbit Γ; this is best seen in the time traces in the right column of figure 10. In the limit one obtains the EtoP heteroclinic cycle shown in figure 11 at the intersection point $(\nu_1, \nu_2) = (0.742526, -1.45729)$ of c_b and the upper curve t_b. Figure 11(a) shows the complete EtoP cycle from Γ to b (black) and back to Γ (grey) in (u, v, w)-space. The computed codimension-one and codimension-zero connections and their time traces are shown in rows (b) and (c), respectively.

Our calculations of the curves c_b and t_b allow us to bring out the missing ingredients of the two-dimensional nature of the accumulation process in the (ν_1, ν_2)-plane, which was already suggested by the oscillating nature of the curve h_1^b in [22]. Indeed, our numerical observations strongly suggest a close link between the details of the accumulation process of the homoclinic orbit and the tangency bifurcations. Note that existing analytical results only deal with the accumulation of points of a homoclinic connection on an EtoP heteroclinic cycle along a one-dimensional curve in parameter space [33].

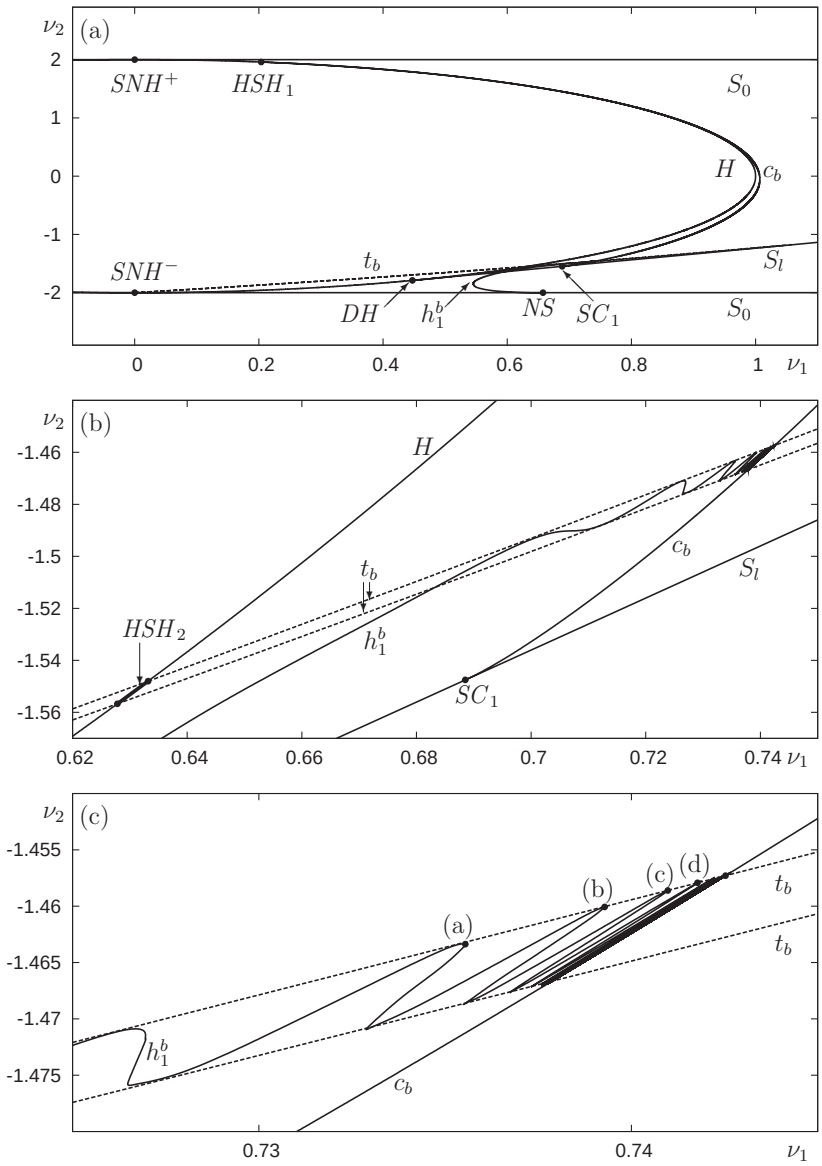

Figure 9. The bifurcation diagram of (26) from figure 6 completed by the curve c_b of codimension-one EtoP connection from b to Γ, and the curves t_b of tangency bifurcation of the codimension-zero connection from Γ back to b. Panel (a) is an overview, and panels (b) and (c) show successive enlargements near the accumulation of h_b^1 onto c_b. Phase portraits and time plots of the orbits at labels (a)-(d) in panel (c) are shown in figure 10, panels (a)-(d). The orbit at the indicated intersection point between c_b and t_b is shown in figure 11.

4.2.2. Accumulation of an EtoP connection By starting from $(\nu_1, \nu_2) = (0.66, -1.558)$ and following the steps shown in section 3 it is possible to find a different EtoP connection between Γ and b than that discussed in section 4.2.1. The

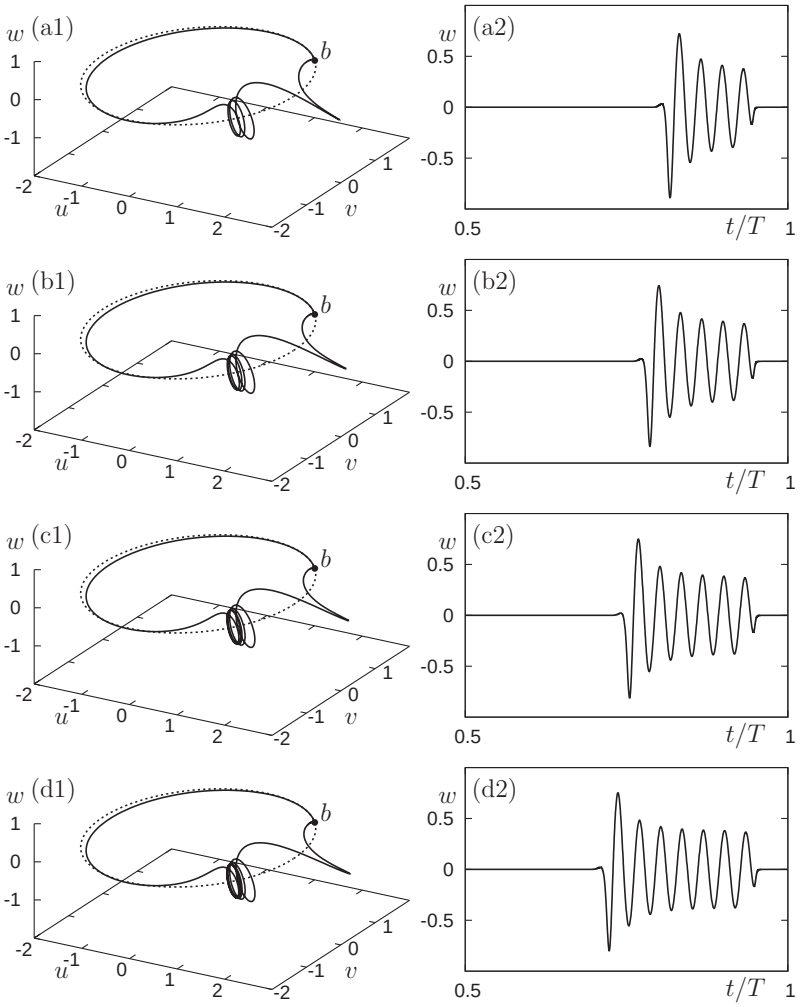

Figure 10. The homoclinic orbit to b of (26) for selected points along the curve h_1^b as indicated in figure 9(c). Shown are the orbits in (u, v, w)-space (left column) and the w-value of the approximating orbit segment (right column) for $(\nu_1, \nu_2) = (0.735540, -1.46337)$ (a), $(\nu_1, \nu_2) = (0.739280, -1.46007)$ (b), $(\nu_1, \nu_2) = (0.740976, -1.45861)$ (c), and $(\nu_1, \nu_2) = (0.741773, -1.45793)$ (d).

continuation of this connection yields the codimension-one curve c_b^* in the bifurcation diagram in figure 12. For decreasing ν_2 the curve c_b^* can be continued past a fold point until it ends at the point SC_2 on S_l. For increasing ν_2 the curve c_b^* appears to accumulate on a segment of c_b; see figure 12(c). It turns out that this accumulation process is associated with a codimension-zero homoclinic orbit to Γ, that is, an intersection of the two-dimensional manifolds $W^u(\Gamma)$ and $W^s(\Gamma)$. The homoclinic

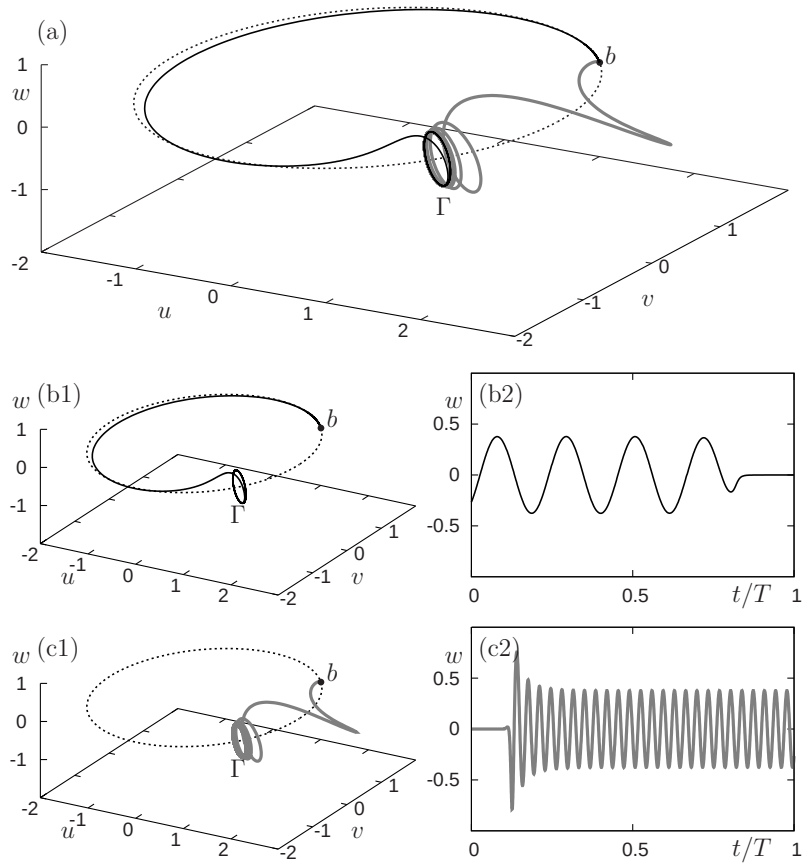

Figure 11. The EtoP heteroclinic cycle of (26) on c_b for $(\nu_1, \nu_2) = (0.742526, -1.45729)$ (a). Panels (b1) and (b2) show the codimension-one EtoP connection and its w-time plot, and panels (c1) and (c2) the codimension-zero EtoP connection and its w-time plot.

orbit to Γ can be found numerically, using the numerical data of the homoclinic orbit to the equilibrium a and continuation through the Hopf bifurcation of a. It exists in a parameter region that is bounded by curves t_Γ where $W^s(\Gamma)$ and $W^u(\Gamma)$ are tangent. The curves t_Γ can also be calculated (using the boundary value problem (24a)–(24c)) and are shown in figure 12 (grey curves) as part of the bifurcation diagram in the (ν_1, ν_2)-plane. For decreasing ν_1 the tangency curves t_Γ end at a Shilnikov-Hopf bifurcation point of equilibrium a; see [20]. For increasing ν_1 the curves t_Γ can be continued until they connect with S_l (not shown).

As figure 12 shows, we have found an accumulation phenomenon of a curve of

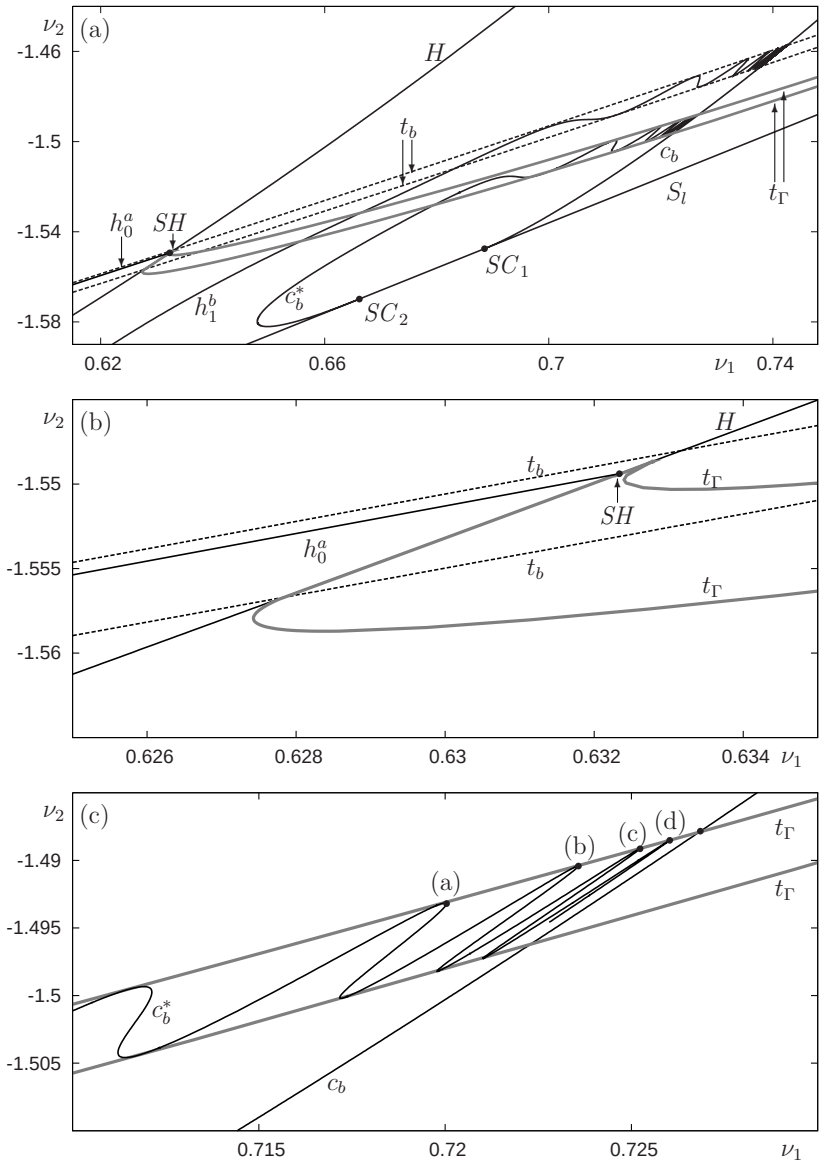

Figure 12. The bifurcation diagram of (26) from figure 9 completed by the curves c_b^* of codimension-one EtoP connections from b to Γ, and the curves t_Γ of tangency bifurcations of the codimension-zero homoclinic connection to Γ. Panel (a) is an overview, panel (b) is an enlargement of the area around the point *SH* where the homoclinic connection to Γ is born, and panel (c) shows an enlargement near the accumulation of c_b^* onto c_b. The computation stops at the endpoint of c_b^* closest to c_b. The orbits at the labels (a)-(d) in panel (c) are shown in figure 13. The orbits at the indicated intersection point of c_b and t_Γ are shown in figure 14.

connecting orbits, but this time of a curve of EtoP connection. Note that the curve c_b^* also enters the region between the tangency curves t_Γ and then appears to oscillate

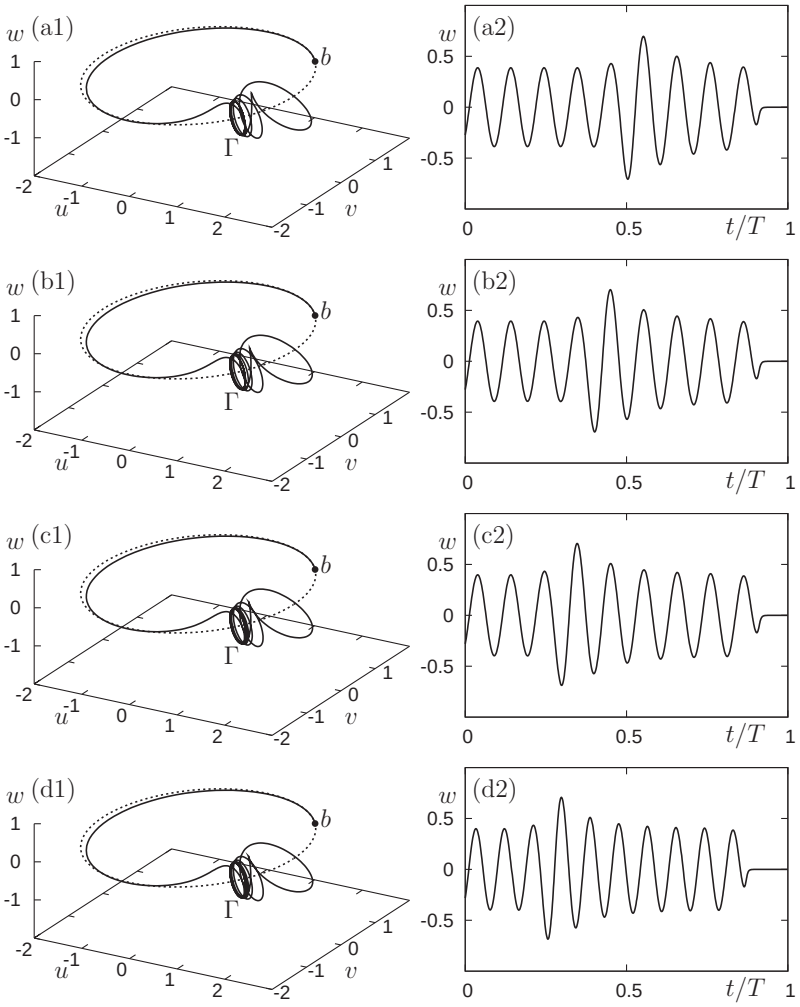

Figure 13. The EtoP connection from Γ to b of (26) for selected points along the curve c_b^* as indicated in figure 12(c). Shown are the orbits in (u, v, w)-space (left column) and the time plot of the approximating orbit segment (right column) for $(\nu_1, \nu_2) = (0.720036, -1.49320)$ (a), $(\nu_1, \nu_2) = (0.723578, -1.49042)$ (b), $(\nu_1, \nu_2) = (0.725231, -1.48914)$ (c), and $(\nu_1, \nu_2) = (0.726028, -1.48852)$ (d). The orbits stay near Γ (note that the number of turns here is only due to the setup of the projection boundary conditions and not related to the accumulation process) before taking one excursion along the homoclinic orbit to Γ, then stay near Γ again, where the number of turns increases by one for each consecutive oscillation of c_b^*, before finally connecting to b.

in between these two curves. Figure 13 shows the respective EtoP connections of successive maxima (w.r.t. ν_1) along the curve c_b^* as indicated in figure 12(c). The

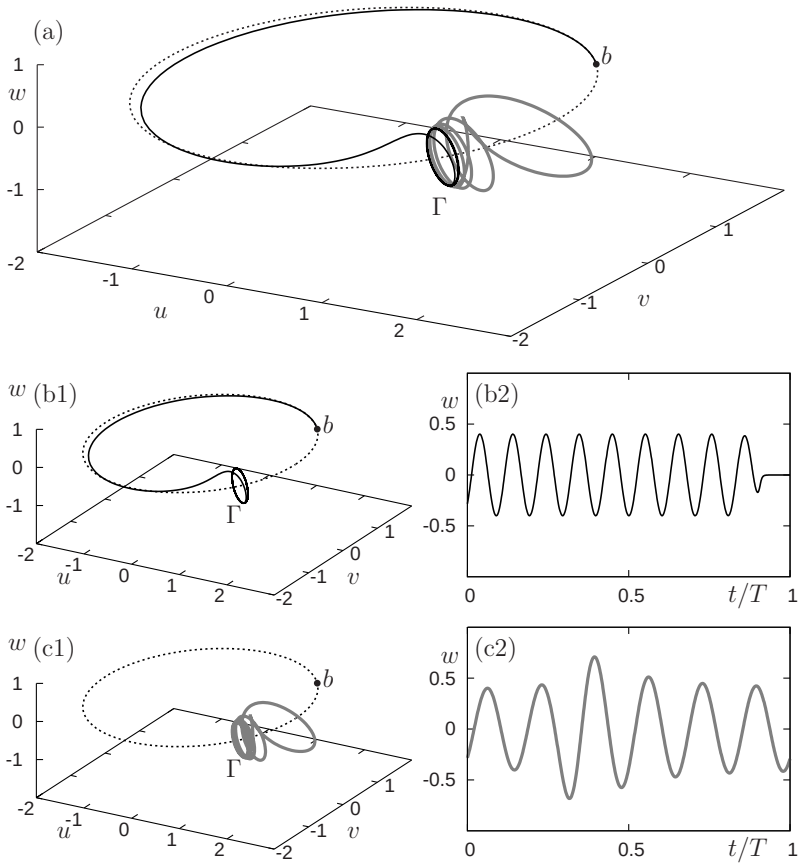

Figure 14. The EtoP connection and the homoclinic orbit to Γ (grey line) of (26) on c_b for $(\nu_1, \nu_2) = (0.726851, -1.48784)$ (a). The EtoP heteroclinic cycle of (26) on c_b for $(\nu_1, \nu_2) = (0.742526, -1.45729)$ (a). Panels (b1) and (b2) show the codimension-one EtoP connection and its w-time plot, and panels (c1) and (c2) the codimension-zero homoclinic connection to Γ and its w-time plot.

EtoP connection departs from Γ, makes one excursion along the homoclinic orbit to Γ, stays near Γ again before finally connecting to b. From maximum to maximum of c_b^* the corresponding EtoP connection from the periodic orbit Γ to b makes one more turn around Γ after the excursion along the homoclinic orbit; this is best seen in the time traces in the right column of figure 13. (Note that the number of turns near Γ before the excursions is due to the projection boundary condition; it is not related to the accumulation process.) The EtoP connection accumulates in the limit on the concatenation of the (different) EtoP connection along c_b and a homoclinic orbit of

Γ. This limiting global object is shown in figure 14; it corresponds to the intersection point $(\nu_1, \nu_2) = (0.726851, -1.48784)$ of c_b and the upper curve t_Γ. Figure 14(a) shows the complete object in (u, v, w)-space, which consists of the homoclinic part from Γ back to Γ (grey curve) and the EtoP connection from Γ to b (black curve) in (u, v, w)-space. The computed codimension-one and codimension-zero connections and their time traces are shown in rows (b) and (c), respectively.

Overall, figure 12 to figure 14 show a new example of the accumulation of a curve of global bifurcations in parameter space. We emphasize that no analytical results exist for this case. The main ingredient is again the fact that the connecting orbit increasingly 'loops around' a periodic orbit of saddle-type, which gives rise in the limit to a concatenation of a codimension-one connection with a codimension-zero connection. We conjecture that this general mechanism underlies the accumulation phenomenon of connecting orbits for vector fields in $\mathbb{R}^3$.

4.3. Codimension-two EtoP connection in a coupled Duffing system

Our method also works in the quite challenging situation that one wants to detect and subsequently continue an EtoP connection of higher codimension. This means that the Lin space is more than one dimensional. As an example we consider here a codimension-two EtoP connection in a four-dimensional coupled Duffing system. This system was derived in [27] as a system with Shilnikov-type homoclinic orbits; it is given as the vector field

$$\begin{cases} \dot{x}_1 &= x_2, \\ \dot{x}_2 &= (a + y_2)x_1 - x_1^3 + \varepsilon(\alpha + \beta y_1)x_2, \\ \dot{y}_1 &= y_2 - \frac{x_1^2}{2}, \\ \dot{y}_2 &= \varepsilon(-y_1 + \gamma y_2 + \lambda y_1^2 y_2). \end{cases} \tag{28}$$

In [27] it was shown that (28) has Shilnikov-type homoclinic orbits to the origin $\mathbf{0}$ for $\lambda = -4\gamma$ and $2a\alpha + (2a\beta + 3)(1 - \sqrt{a}) = 0$, $0 < a < 1$, $\gamma > 0$. Therefore we also expect to find EtoP connections in this system. We fix $a = 0.0461071$, $\gamma = 2.63680$ and $\lambda = -27.6186$ and consider ε, α and β as continuation parameters. Specifically, we start the first step of our method from

$$\varepsilon = 0.0881558,\ \beta = 15.0,\ \alpha = -5.17613.$$

The eigenvalues of the Jabobian at $\mathbf{0}$ are given by

$$\frac{1}{2}\alpha\varepsilon \pm \sqrt{\frac{1}{4}\alpha^2\varepsilon^2 + a} \quad \text{and} \quad \frac{1}{2}\varepsilon\gamma \pm \sqrt{\frac{1}{4}\varepsilon^2\gamma^2 - \varepsilon}.$$

Throughout the parameter region we are considering $\mathbf{0}$ has one negative eigenvalue and three eigenvalues with positive real part. Hence, $W^s(\mathbf{0})$ is of dimension one. Moreover, there is a saddle-type periodic orbit Γ, which can be found by continuatiuon from a Hopf bifurcation of one of the secondary equilibria of (28). In the parameter region of interest Γ has two stable Floquet multipliers and one unstable Floquet multiplier. Hence, $W^u(\Gamma)$ is of dimension two.

We are seeking here the codimension-two EtoP connection from Γ to $\mathbf{0}$ that exists when $W^s(\mathbf{0}) \subset W^u(\Gamma)$. Since the connection is from Γ to b, time needs to be reversed when formulating the respective boundary value problems from section 3. We remark that the unstable Floquet multiplier of Γ is actually negative, which means that $W^u(\Gamma)$ is non-orientable.

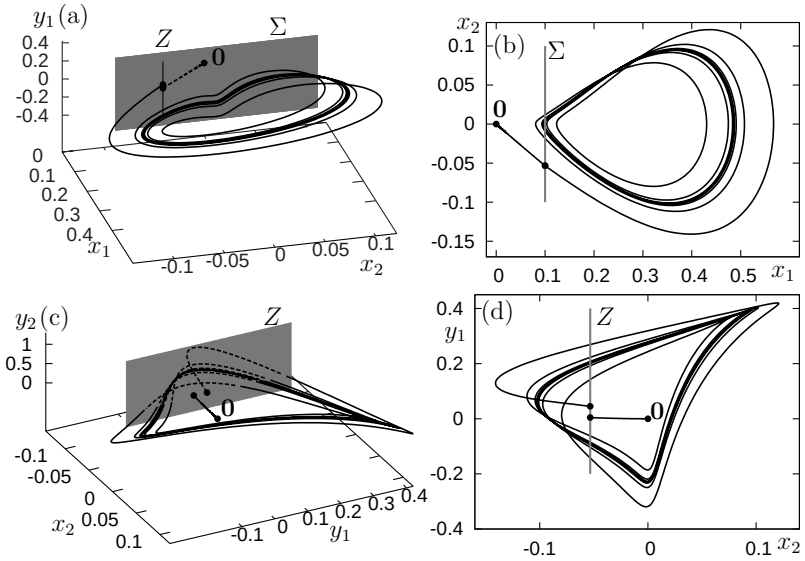

Figure 15. The orbit segments from Γ to Σ and from Σ to **0** of (28) for $\varepsilon = 0.0881558$, $\beta = 15.0$ and $\alpha = -5.17613$, shown in projection onto (x_1, x_2, y_1)-space (a) and onto the (x_1, x_2)-plane (b). The end points of both orbit segments in Σ actually lie in the two-dimensional Lin plane Z, as is shown in projection onto (x_1, x_2, y_2)-space (c) and onto the (x_2, x_1)-plane (d).

One end point of the orbit segment u^+ starting from near **0** lies in $E^s(\mathbf{0})$. We choose a mesh point $g \in \Gamma$, namely the point

$$g = \begin{pmatrix} x_1 \\ x_2 \\ y_1 \\ y_2 \end{pmatrix} = \begin{pmatrix} 0.0969620 \\ -0.00183236 \\ -0.228516 \\ 0.0000130318 \end{pmatrix}.$$

One end point of the orbit segment u^- starting near Γ is then chosen to lie at distance δ from g on the corresponding Floquet vector v at g. Integration by continuation as described in section 3.2 can be used to extend the orbit segments u^+ and u^- so that their other end points lie in the fixed section

$$\Sigma := \{x_1 = 0.1\}.$$

Figure 15 shows different projections of the orbit segments u^+ from Σ to **0** and u^- from Γ to Σ. Note that Σ is three dimensional but, due to the chosen projections, it appears as a plane and as a line in figure 15(a) and (b), respectively. For computational convenience and for the sake of clear illustrations we chose the two-dimensional Lin space Z parallel to the (y_1, y_2)-plane. Figure 15(c) and (d) are two different projections that show Z as a plane and as a line, respectively. Note that the distance δ along the Floquet vector v has been chosen such that the difference $u^+(0) - u^-(1)$ already lies in the Lin space Z; cf. section 3.3.

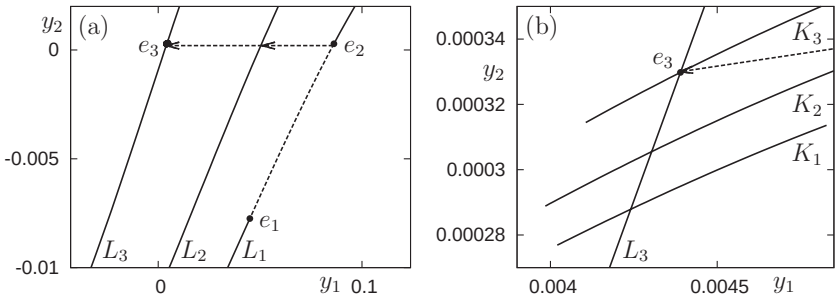

Figure 16. The curves L_i and K_i are traced out in the Lin plane Z by the end points of orbit segements during continuation in the gap sizes η_1, η_2 and the system parameter ε. Namely the L_i are traced out by the orbit segment u^- from Γ to Σ, and the K_i by the orbit segment u^+ from Σ to $\mathbf{0}$; here L_1 and K_1 are for $\alpha = \alpha_1 = -5.17613$, L_2 and K_2 are for $\alpha = \alpha_2 = -4.86955$, and L_3 and K_3 are for $\alpha = \alpha_3 = -4.5$. The enlargement in panel (b) indicates that the K_i change only very little with the system parameters. To close the gap we start from e_1 and follow L_1 until $\eta_1 = 0$ at e_2. Then we continue in η_2 and the system parameters ε and α until $\eta_2 = 0$, which happens at the point $L_3 \cap K_3 = e_3$.

Given the choice of Z it is natural to measure the Lin gaps η_1 and η_2 along the y_1 and y_2 coordinate directions, respectively. The initial gap sizes are $\eta_1 = -0.0405882$ and $\eta_2 = 0.00803835$. In order to close the two gaps, we first continue in η_1, η_2 and the system parameter ε; cf. section 3.4, $(22a)$–$(22n)$. The end points inside Z of the orbit segments that are computed during the continuation are depicted in figure 16. Namely, the end points of the orbit segments u^- from Γ to Σ trace out the curve L_1 shown in figure 16(a). At the same time, the end points of the orbit segment u^+ from Σ to $\mathbf{0}$ trace out a curve K_1. In fact, the point u^+ hardly changes and the curve K_1 is visible only in the enlarged figure 16(b). The curves L_1 and K_1 (which are parametrized by the system parameter ε) are for $\alpha = \alpha_1 = -5.17613$. Also shown in figure 16 are the curves L_2, L_3, K_2 and K_3 for $\alpha = \alpha_2 = -4.86955$ and for $\alpha = \alpha_3 = -4.5$, respectively. The curves L_i and K_i, $i = 1, 2, 3$, show that the Lin plane Z is locally given by two one-parameter families of unique one-dimensional curves that intersect transversely. In other words, the gap can be closed in a systematic way. Namely, we first continue in η_1, η_2 and ε starting at the point e_1 along L_1 until a $\eta_2 = 0$ is detected; see the point e_2 in figure 16(a). We then fix $\eta_2 = 0$ and change to a continuation in η_1, ε and α. The continuation traces out the (almost) horizontal dashed line in figure 16(a) and stops when a zero of η_1 is detected, which happens for $\varepsilon = 0.1$ and $\alpha = -4.5$. In the enlargement figure 16(b) this occurs at the intersection of L_3 and K_3, denoted by e_3.

Once both Lin gaps have been closed, that is, $\eta_1 = \eta_2 = 0$, we have found a codimension-two EtoP connection from Γ to $\mathbf{0}$. The connecting orbits can now be continued in the three system parameters ε, β and α. Figure 17(a) and (b) shows the resulting curve h of connecting orbits in $(\varepsilon, \alpha, \beta)$-space and in projection onto the (ε, β)-plane, respectively. We remark that the curve h does not self-intersect, even though one may get this impression due to projection. Five points along h are labelled and the respective connecting orbits are shown in figure 17(c)–(g) in (x_1, x_2, y_1)-space and as a times series of the norm. Notice how the connecting orbits changes along the curve h. In figure 17(c) the connection follows Γ closely and then quickly connects

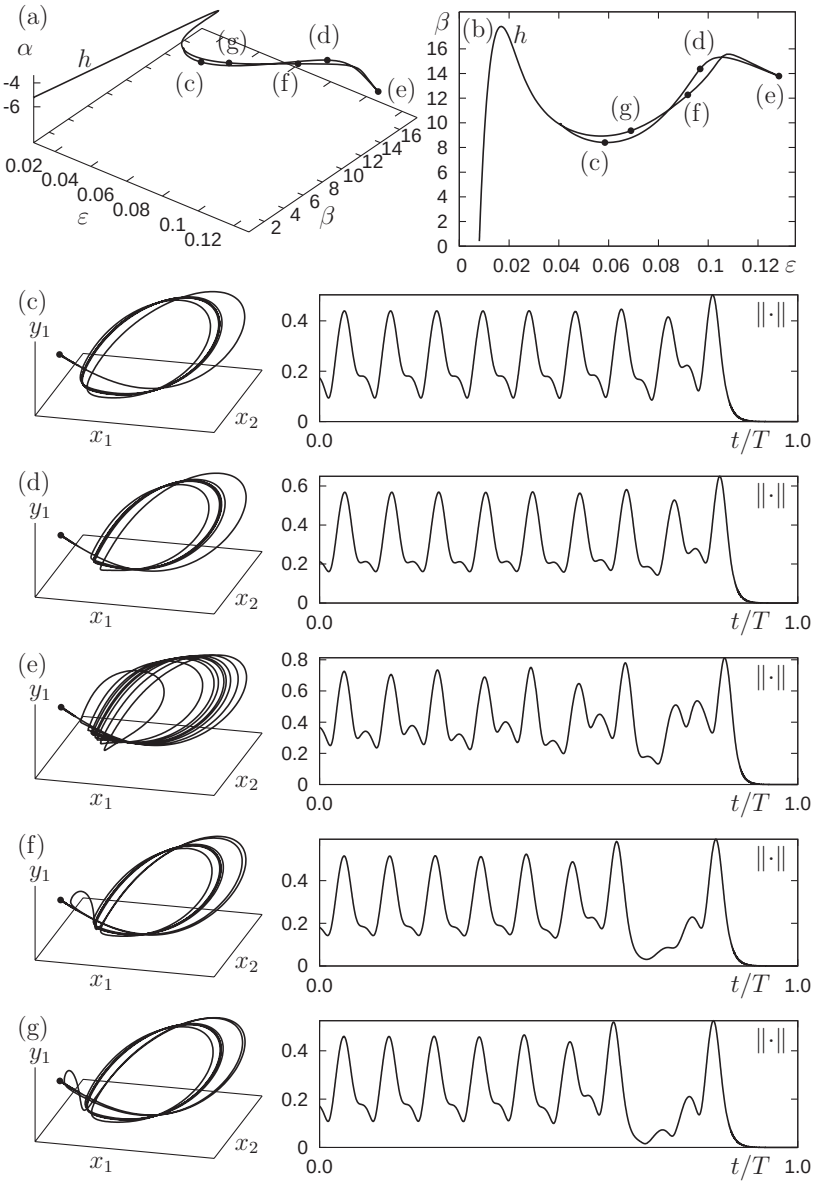

Figure 17. The curve h of codimension-two EtoP connections of (28) shown in $(\varepsilon, \alpha, \beta)$-space (a) and in projection onto the (ε, β)-plane (b). Rows (c)–(g) show selected connecting orbits, as indicated along h, in (x_1, x_2, y_1)-space and as time series of the norm; namely, from (c) to (g) $(\varepsilon, \alpha, \beta)$ has the values $(0.0584877, -3.51797, 8.40132)$, $(0.0967731, -4.25440, 14.3715)$, $(0.128392, -4.59897, 13.7927)$, $(0.0918179, -3.71152, 12.2683)$, and $(0.0689425, -3.46446, 9.36032)$.

to **0**. This gradually changes and the connecting orbit makes a closer and closer pass near **0** and then makes another large excursion before it connects to **0**; see figure 17(f) and (g). We remark that the curve h could not be computed beyond what is shown in figure 17(a) and (b). It appears that this is due to the connecting orbit passing very close to **0** at an intermediate point. In the limit, it seems that the connection becomes a concatenation of a new codimension-two connection from Γ to **0** and a codimension-one homoclinic orbit from **0** back to itself. A more detailed study of the global bifurcations of (28) is beyond the scope of this paper, but we remark that a similar phenomenon has been found for codimension-zero EtoP connections in the Lorenz system [14].

5. Finding PtoP connections

It is quite straightforward to generalize our approach for finding EtoP connections to the case of codimension-d PtoP connections from one periodic orbit Γ_1 to another periodic orbit Γ_2. Suppose that $\dim(W^u(\Gamma_1)) = k \geq 2$, $\dim(W^s(\Gamma_2)) = l \geq 2$, and that these manifolds intersect in an isolated orbit that is generic (in the sense of (C4) from section 2). We consider two orbit segments u^- from Γ_1 to a suitable section Σ, and u^- from Σ to Γ_2 subject to the boundary conditions

$$u^-(0) = u^1_\gamma(0) + \sum_{i=1}^{k-1} \varepsilon_i u^1_i(0), \tag{29a}$$

$$u^+(1) = u^2_\gamma(0) + \sum_{i=1}^{l-1} \delta_i u^2_i(0), \tag{29b}$$

$$\left\langle u^-(1) - p_\Sigma, n_\Sigma \right\rangle = 0, \tag{29c}$$

$$(u^+(0) - u^-(1)) = \sum_{i=1}^{d} \eta_i(\lambda) z_i, \tag{29d}$$

where the vectors z_i are again a basis of a suitably chosen d-dimensional Lin space; the numerical representations of Γ_1 and Γ_2 are denoted by u^1_γ and u^2_γ, respectively, the representations of the associated unstable and stable eigenfunctions are denoted by u^1_i and u^2_i.

The geometry of a PtoP connection is very similar to that of a EtoP connection, and we strongly believe that the equivalent statement of theorem 2.1 can be proved for PtoP connections. While technical details need to be checked to prove this conjecture, it appears quite clear that the two orbit segments are uniquely determined by choosing a d-dimensional Lin space. In other words, the general setup given by (29*a*)–(29*d*), in combination with the continuation of u^1_γ with its unstable eigenspace u^1_i and of u^2_γ with its stable eigenspace u^2_i, constitutes a well-defined boundary value problem. In particular, closing the test functions $\eta_i(\lambda)$ one by one provides a systematic way of finding a codimension-d PtoP connection.

We remark that it is not at all straighforward to find a numerical example of a codimension-d PtoP connections for $d \geq 1$. Even identifying a candidate vector field among models from applications is quite a task, as it requires finding two saddle periodic orbits with the correct dimensions of their stable and unstable manifolds. Therefore, we now discuss the problem of continuing a robust PtoP connection of codimension zero. In section 4.1 and in section 4.2 we have actually already seen

two examples, namely for the case that the connection is a homoclinic orbit from a periodic orbit Γ back to itself. As was explained in section 3.5, an initial homoclinic PtoP connection can be found from the concatenated data of a EtoP heteroclinic cycle consisting of a codimension-one and a codimension-zero EtoP connection. The homoclinic PtoP can then be continued imposing projection boundary condition (24*b*) and (24*c*) at Γ at both ends of the connecting orbit segment u.

Consider now a codimension-zero PtoP connection between two different saddle periodic orbits Γ_1 and Γ_2 of periods T_1 and T_2, respectively. Indeed it is possible to approximate this PtoP connection also with a single orbit segment u subject to projection boundary condition at both Γ_1 and Γ_2, which is the approach taken in [9]. The problem is that for PtoP connections there is no simple way to construct an initial approximate connecting orbit segment. As an alternative we propose the following geometric approach. We assume that the codimension-zero PtoP connection is generic, which means that $l + k = n + 1$, the Lin space is trivial, and $d = 0$ in (29*d*). We fix the system parameter λ and, as for the general method above, perform step 1 of constructing the orbits segments u^- and u^+ by continuation in the integration time T, so that $u^-(1) \in \Sigma$ and $u^+(0) \in \Sigma$. This means that u^- and u^+ satisfy (29*a*)–(29*c*), but not (29*d*) since $u^+(0) - u^-(1) \neq 0$. Recall that the Lin space is trivial, so that the difference $u^+(0) - u^-(1)$ can be chosen to be zero without changing the system parameter λ. To achieve this, we set $z_0 := (u^+(0) - u^-(1))/\,\|u^+(0) - u^-(1)\|$ and define the one-dimensional subspace $Z_0 := \mathrm{span}\{z_0\}$. Replacing condition (29*d*) by

$$(u^+(0) - u^-(1)) = \eta\, z_0 \tag{30}$$

ensures that the difference $u^+(0) - u^-(1)$ remains restricted to Z_0. As a result, the overall boundary problem given by (29*a*)–(29*c*), (30), together with the respective formulations for Γ_1 with its unstable eigenspace and of Γ_2 with its stable eigenspace, is well posed, meaning that T_1, T_2, ε_i, δ_j, and η are uniquely defined. Hence, $\eta = \eta(T_1, T_2, \varepsilon_i, \delta_j)$ is a well-defined test function, so that a continuation run in the direction of decreasing η allows us to find the codimension-zero PtoP connection as a zero of η.

5.1. Codimension-zero PtoP connection in a four-dimensional vector field

As an example of a system with a codimension-zero PtoP connection we consider the four-dimensional system considered in [9]. It is given by

$$\left\{\begin{array}{lcl} \dot{x} &=& (1-w)y + wx\left(1-x^2\right), \\ \dot{y} &=& (1-w)\left(-x + \lambda(1-x^2)y\right) + w\left(z-3-\lambda\right), \\ \dot{z} &=& (1-w)z\left(z^2 - (4+\lambda)^2\right) \\ && +w\left(-y+3+\lambda+\lambda\left(1-(y-3-\lambda)^2\right)(z-3-\lambda)\right), \\ \dot{w} &=& w(1-w), \end{array}\right. \tag{31}$$

where the parameter λ is set to $\lambda = 0.5$. System (31) can be interpreted as a homotopy from $w = 0$ to $w = 1$ between two planar systems in the (x, y)-plane and in the (y, z)-plane, respectively. In each of the two planes the system resembles a Van der Pol oscillator with an attracting periodic orbit. We denote the periodic orbit in the (x, y)-plane by Γ_1 and the one in the (y, z)-plane by Γ_2. Since $\dim W^u(\Gamma_1) = 2$ and $\dim W^s(\Gamma_2) = 3$ one expects a codimension-zero PtoP connection from Γ_1 to Γ_2. In [9] this PtoP connection was found with difficulties by using a shooting technique and then continued in λ.

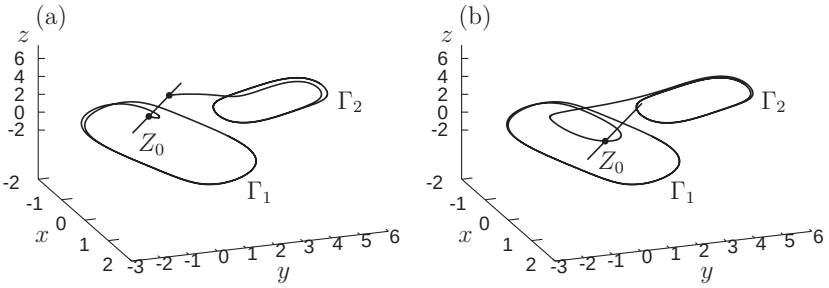

Figure 18. Orbit segments $u^- \subset W^u(\Gamma_1)$ and $u^+ \subset W^s(\Gamma_2)$ up to the section $\Sigma = \{w = 0.5\}$ of (31) for $\lambda = 0.5$. Their end points $u^-(1), u^+(0) \in \Sigma$ are restricted to lie in the direction Z_0. The gap η is initially nonzero (a), and is then closed by a continuation run to reveal a codimension-zero PtoP connection (b). Note that only Z_0 of the section Σ appears in the panels due to the chosen projection.

We choose the cross-section to be $\Sigma = \{w = 0.5\}$ which clearly separates the two periodic orbits. As base points on Γ_1 and Γ_2 we use

$$g_1 = \begin{pmatrix} 0.0 \\ 5.28342 \\ 4.60521 \\ 1.0 \end{pmatrix}, \quad g_2 = \begin{pmatrix} -0.0131541 \\ 2.03745 \\ 0.0 \\ 0.0 \end{pmatrix}.$$

Furthermore, we compute the (fixed) Floquet vectors at these points for the definition of the projection boundary conditions (29a) and (29b). After computing the orbit segments u^- and u^+ up to Σ, we construct the one-dimensional space Z_0 from $u^+(0) - u^-(1)$ and find that the distance η in (30) is $\eta = 3.76668$; see figure 18(a). Continuation of the overall boundary value problen in T_1, T_2, ε_1, δ_1, δ_2 and η then detects the codimension-zero PtoP connection shown in figure 18(b) as a zero of η.

6. Conclusions and outlook

We presented a method based on Lin's method that allows one to find a generic codimension-d EtoP connection from a saddle equilibrium to a saddle periodic orbit. The key idea is to set up an overall boundary value problem that defines two separate orbit segments up to a specified cross section, whose end points lie in a well-defined d-dimensional space. The two orbit segments exist in an entire region of parameter space (and not just at the heteroclinic connection), so that they give rise to d smooth test function, known as the Lin gaps. Closing the Lin gap in consecutive continuation runs allows one to find codimension-d EtoP connections in a systematic way. The EtoP connection and related global objects, such as homoclinic orbits of the periodic orbit, can then be continued in system parameters. We demonstrated with three example vector fields how our method for finding EtoP connections can be used to investigate quite complicated bifurcation phenomena.

The study of EtoP connections in other vector field models from applications is an obvious direction for future research; interesting candidates are laser models [40], models from cell dynamics [6], or models for voltage collapse in power systems [1].

We also presented a general setup for finding codimension-d PtoP connections. While the underlying statement of Lin's method has not been proved, geometrical arguments strongly suggest that the respective Lin gaps are regular test functions. Furthermore, we showed with the example of a vector field in $\mathbb{R}^4$ how a generic codimension-zero PtoP connection can be found in practice. The demonstration of the method for codimension-d PtoP connections for $d > 0$ remains a challenge for the future, not in the least due to the difficulty of finding vector fields with PtoP connections. On the theoretical side, an extension to Lin's method to PtoP connections is desirable as a foundation of the presented general setup.

Acknowledgements

We thank Jürgen Knobloch, Bart Oldeman and Hinke Osinga for helpful discussions. T.R. acknowledges the hospitality of and financial support from the Bristol Centre for Applied Nonlinear Mathematics at the Department of Engineering Mathematics, University of Bristol, during two long research visits in 2006 and 2007; he also acknowledges the support from the Department of Technical Mechanics of the Faculty of Mechanical Engineering, TU Ilmenau, in 2006 and 2007.

References

[1] Abed E H, Wang H O, Alexander J C, Hamdan A M A and Lee H-C 1993 Dynamic bifurcations in a power system model exhibiting voltage collapse *Int. J. Bif. and Chaos* **3** 1169–76

[2] Ashwin P, Rucklidge A M and Sturman R 2004 Two-state intermittency near a symmetric interaction of saddle-node and Hopf bifurcations: a case study from dynamo theory *Physica D* **194** 30–48

[3] Beyn W-J 1994 On well-posed problems for connecting orbits in dynamical systems *Cont. Math. Chaotic Numerics* **172** 131–68

[4] Beyn W-J 1990 The numerical computation of connecting orbits in dynamical systems *IMA J. Numer. Anal.* **10** 379–405

[5] Champneys A R, Kuznetsov Yu A and Sandstede B 1996 A numerical toolbox for homoclinic bifurcation analysis *Int. J. Bif. and Chaos* **6** 867–87

[6] Champneys A R, Kirk V, Knobloch E, Oldeman B E and Sneyd J 2007 When Shil'nikov Meets Hopf in Excitable Systems *SIAM J. Appl. Dynam. Syst.* **6** 663–93

[7] Demmel J W, Dieci L and Friedman M J 2000 Computing connecting orbits via an improved algorithm for continuing invariant subspaces *SIAM J. Sci. Comput.* **22** 81–94

[8] Dercole F 2007 BPcont: an Auto97 driver for the continuation of branch points of algebraic and boundary-value problems; presented at *CRM workshop Advanced Algorithms and Numerical Software for the Bifurcation Analysis of Dynamical Systems* July 2007

[9] Dieci L and Rebaza J 2004 Point-to-periodic and periodic-to-periodic connections *BIT Numerical Mathematics* **44** 41–62

[10] Dieci L and Rebaza J 2004 Erratum: Point-to-periodic and periodic-to-periodic connections *BIT Numerical Mathematics* **44** 617–18

[11] Doedel E J 2007 Lecture notes on numerical analysis of nonlinear equations, in Krauskopf B, Osinga H M and Galán-Vioque J (Editors) 2007 *Numerical Continuation Methods for Dynamical Systems* (Springer)

[12] Doedel E J and Friedman M J 1989 Numerical computation of heteroclinic orbits *J. Comput. Appl. Math.* **26** 155–70

[13] Doedel E J, Kooi B W, Kuznetsov Yu A and Voorn G A K 2007 Continuation of connecting orbits in 3D-ODES: (I) Point-to-cycle connections *Preprint* arXiv:0706.1688D

[14] Doedel E J, Krauskopf B and Osinga H M 2006 Global bifurcations of the Lorenz manifold *Nonlinearity* **19** 2947–72

[15] Doedel E J, Pfaffenroth R C, Champneys A R, Fairgrieve T F, Kuznetsov Yu A, Oldeman B E, Sandstede B and Wang X J 2000 AUTO 2000: Continuation and bifurcation software for ordinary differential equations *Technical report* `http://cmvl.cs.concordia.ca`

[16] Doedel E J, Pfaffenroth R C, Champneys A R, Fairgrieve T F, Kuznetsov Yu A, Oldeman B E, Sandstede B, Wang X J and Zhang C 2006 AUTO-07P: Continuation and bifurcation software for ordinary differential equations *Technical report* `http://cmvl.cs.concordia.ca`

[17] England J P, Krauskopf B and Osinga H M 2005 Computing one-dimensional global manifolds of Poincaré maps by continuation *SIAM J. Appl. Dynam. Syst.* **4** 1008–41

[18] Friedman M J and Doedel E J 1993 Computational methods for global analysis of homoclinic and heteroclinic orbits: A case study *J. Dyn. and Diff. Eq.* **5** 37–57

[19] Guckenheimer J and Holmes P 1983 *Nonlinear Oscillations, Dynamical Systems, and Bifurcations of Vector Fields* (*Applied Mathematical Sciences* vol 42) (New York: Springer)

[20] Hirschberg P and Knobloch E 1993 Šil'nikov-Hopf bifurcation *Physica D* **62** 202–16

[21] Knobloch J 2004 Lin's Method for Discrete and Continuous Dynamical Systems and Applications *Habilitationsschrift* TU Ilmenau

[22] Krauskopf B and Oldeman B E 2006 Bifurcations of global reinjection orbits near a saddle-node Hopf bifurcation *Nonlinearity* **19** 2149–67

[23] Krauskopf B, Osinga H M and Galán-Vioque J (Editors) 2007 *Numerical Continuation Methods for Dynamical Systems* (Springer)

[24] Krauskopf B, Tollenaar N and Lenstra D 1998 Tori and their bifurcations in an optically injected semiconductor laser *Optics Communications* **156** 158–69

[25] Kuznetsov Yu A 1998 *Elements of applied bifurcation theory (3rd ed.)* (*Applied Mathematical Sciences* vol 112) (New York: Springer)

[26] Lentini M and Keller H B 1980 Boundary Value Problems on Semi-Infinite Intervals and Their Numerical Solution *SIAM J. Num. Anal.* **17** 577–604

[27] Li W and Xu P 2003 The Existence of Silnikov's Orbit in Four-dimensional Duffing's Systems *AMAS* 19 **4** 677–90

[28] Lin X-B 1990 Using Melnikov's method to solve Shilnikov's problems *Proc. Roy. Soc. Edinburgh* A **116** 295–325

[29] Lorenz E N 1963 Deterministic nonperiodic flows *J. Atmospheric Sci.* **20** 130–41

[30] Lust K 2001 Improved numerical Floquet multipliers *Int. J. Bifurc. Chaos* **11** 2389–410

[31] Oldeman B E, Champneys A R and Krauskopf B 2003 Homoclinic branch switching: a numerical implementation of Lin's method *Int. J. Bifurc. Chaos* **13** 2977–99

[32] Pampel T 2001 Numerical approximation of connecting orbits with asymptotic rate *Numerische Mathematik* **90** 309–48

[33] Rademacher J D 2005 Homoclinic orbits near heteroclinic cycles with one equilibrium and one periodic orbit *J. Diff. Eq.* **218** 390–443

[34] Rieß T 2003 Using Lin's method for an almost Shilnikov problem *Diploma Thesis* TU Ilmenau

[35] Sandstede B 1993 Verzweigungstheorie homokliner Verdopplungen *Dissertationsschrift* Universität Stuttgart

[36] Sparrow C 1982 *The Lorenz Equations: Bifurcations, Chaos and Strange Attractors* (*Applied Mathematical Sciences* vol 41) (New York: Springer)

[37] Strogatz S 1994 *Nonlinear Dynamics and Chaos: With Applications to Physics, Biology, Chemistry and Engineering* (Reading, MA: Addison-Wesley)

[38] Vitolo R 2003 Bifurcations of attractors in 3D diffeomorphisms: a study in experimental mathematics *PhD Thesis* University of Groningen

[39] Wieczorek S M, Krauskopf B, Simpson T B and Lenstra D 2005 The dynamical complexity of optically injected semiconductor lasers *Physics Reports* **416** 1–128

[40] Wieczorek S M and Krauskopf B 2005 Bifurcations of n-homoclinic orbits in optically injected lasers *Nonlinearity* **18** 1095–120

[41] Yew A C 2001 Multipulses of Nonlinearly Coupled Schrödinger Equations *J. Diff. Eq.* **173** 92–137

[42] Zimmermann M, Natiello M and Solari H 2001 Global bifurcations in a laser with injected signal: beyond Adler's approximation *Chaos* **11** 500–13